# Dual inhibition of EZH2 and EZH1 sensitizes multiple myeloma cells to proteasome inhibition

（EZH1 と EZH2 の同時阻害は多発性骨髄腫細胞のプロテアソーム阻害剤への反応性を亢進させる）

Chiba University Graduate School of
Medical and Pharmaceutical Sciences
Frontier Medicine and Pharmacy
(Chief Prof: Prof. Atsushi Iwama)
**Ola Mohammed Kamel AbdelBassir Helal Rizq**

**Abstract**

Enhancer of zeste homolog 2 (EZH2) and its homolog EZH1, the catalytic components of polycomb repressive complex 2 (PRC2), are methyltransferases that induce the trimethylation of histone H3 at lysine 27 generating H3K27me3, leading to repression of the transcription of target genes. PRC2 components have been implicated in the pathogenesis of different kinds of cancer. Specifically, EZH2 is highly expressed in solid malignancies such as breast, prostate and bladder cancers as well as in multiple myeloma (MM). Overexpression of EZH2 correlated with disease progression and aggressiveness. Recently, several dual EZH2/1 inhibitors have been developed with promising preliminary reports in non-Hodgkin lymphomas (NHLs).

In this study, we investigated the pre-clinical therapeutic efficacy of the combination of UNC1999, a novel EZH2/1 inhibitor, and proteasome inhibitors in PRC2-dependent tumors: multiple myeloma and prostate cancer.

We demonstrated that PRC2 was a valid target for the treatment of MM as evidenced by the growth inhibitory effects of *EZH2* knockdown and dual inhibition of EZH2/1 by UNC1999 on MM cells. Remarkably, MM cells acquired resistance to proteasome inhibition following *EZH2* overexpression using lentiviral vectors. Interestingly, this resistance was overcome by UNC1999. Importantly, we found that proteasome inhibitors downregulated *EZH2* transcription via disruption of Rb-E2F pathway, however, EZH1 was not affected and H3K27me3 mark remained largely unchanged. In vitro as well as in vivo synergistic anti-myeloma effects of the combination of UNC1999 and proteasome inhibitors were illustrated. Remarkably, combining proteasome inhibitors with UNC1999 resulted in a more synergistic effect than with a specific EZH2 inhibitor. This suggested that inhibition of both EZH2 and EZH1 was needed to completely block PRC2 activity in MM cells. Comprehensive genomic analysis uncovered the direct targets of UNC1999 in MM which included the tumor

suppressor *NR4A1*. Activation of *NR4A1* was associated with repression of *MYC*, which was further enhanced by the combination of UNC1999 and proteasome inhibitors. Potent synergistic effect of the combination of UNC1999 and proteasome inhibitors was also observed in prostate cancer cell lines.

Our study provides pre-clinical evidence of the promising therapeutic value of the combination of PRC2 inhibition and proteasome inhibition in the treatment of PRC2-dependent cancers.

## Introduction

Polycomb repressive complex 2 (PRC2) represses the transcription of target genes through its catalytic components: enhancer of zeste homolog 2 (EZH2) and its homolog EZH1, catalyzing trimethylation of H3K27 (H3K27me3) [1]. This repressive mark is removed by the histone demethylases ubiquitously transcribed tetratricopeptide repeat X chromosome (UTX; also known as KDM6A) and jumonji domain-containing protein 3 (JMJD3; also known as KDM6B) [2]. PRC2 is closely linked to the control of stem cells and tumorigenesis [3]. Specifically, EZH2 is frequently deregulated in cancer and its overexpression was reported in solid malignancies such as prostate cancer [4] as well as in hematological malignancies such as lymphoma in which *EZH2*-activating mutations were identified [5], suggesting that EZH2 is a new potential therapeutic target. Indeed, clinical trials of EZH2 inhibitors in a variety of cancers are ongoing [6]. Recently, dual inhibitors of EZH2 and EZH1 have been developed to conquer PRC2-dependent cancers [7,8]. Noteworthy, it was shown that UNC1999 [9], a novel small molecule inhibitor that is active against EZH2 (both wild type and mutant) and EZH1, has a promising pre-clinical activity against *MLL*-rearranged leukemia in vitro and in vivo [7].

Multiple myeloma (MM), which accounts for more than 1% of all cancer deaths [10], remains an incurable disease, thereby emphasizing the need for novel therapeutic approaches to improve patient outcome [11]. In MM, *EZH2* overexpression correlates with the progression from monoclonal gammopathy of undetermined significance (MGUS) to MM [12]. Significantly, the identification of inactivating mutations in *UTX* in 10% of myeloma samples underscores the important role of H3K27me3 in myelomagenesis [13]. Moreover, *EZH2* knockdown using siRNA leads to the inhibition of MM cell growth [14]. These data propose a possible use of EZH2 inhibitors in the treatment of MM. Indeed, a few reports of the use of EZH2 inhibitors in MM have recently emerged with varying degrees of success [15-17]. However, neither detailed molecular mechanisms of action of the novel agents nor the

combination with currently available agents in vitro and in vivo has been thoroughly investigated. In the last decade, proteasome inhibitors such as bortezomib and carfilzomib together with other innovative therapeutics have dramatically improved the life expectancy of MM patients [11]. Despite this breakthrough, patients eventually develop resistance to treatment, therefore combining proteasome inhibitors with novel agents is one option to improve patient outcome [18]. Whether the combination of proteasome inhibitors and novel PRC2 inhibitors constitutes a new therapeutic strategy has not yet been explored.

Prostate cancer, a leading cause of death in men [10], is another malignancy in which EZH2 plays a crucial role through its part as the catalytic unit of PRC2 [4] and also through PRC2-independent co-activation of transcription factors such as androgen receptor [19]. The success of bortezomib in MM increased the interest in using it in non-hematological malignancies [20]. Thus, several phase I/II clinical trials were conducted using bortezomib alone and in combination with other agents for the treatment of prostate cancer; however, these studies reported only moderate to no improvement in patient outcome [21].

In this study, we investigated the potential of the dual inhibition of EZH2 and EZH1 together with proteasome inhibitors as a novel mechanistic approach for the treatment of PRC2-dependent tumors such as MM and prostate cancer.

## Materials and methods

### Human samples from patients and healthy volunteers

MM cells and bone marrow stromal cells (BMSCs) were collected from the bone marrow of newly diagnosed MM patients at Chiba University Hospital. All patients provided written informed consent in accordance with the declaration of Helsinki and patient anonymity was ensured. This study was approved by the Institutional Review Committee at Chiba University (Approval #532). Plasma cells were purified and BMSCs were generated as previously described [22,23]. Peripheral Blood samples collected from healthy volunteers were processed by Ficoll-Paque (GE Healthcare) gradient to obtain peripheral blood mononuclear cells.

### Human cell lines

Human MM cells MM.1S, NCI-H929 (H929) and RPMI8226; human prostate cancer cells LNCaP and DU145; and human embryonic HEK293T cells were obtained from American Type Culture Collection. Human KMS11 and bortezomib-resistant KMS11/BTZ [24] cells were obtained from Japanese Collection of Research Bioresources Cell Bank. Human OPM1 and OPM2 plasma cell leukemia cell lines and doxorubicin-resistant RPMI-DOX40 (DOX40) cells were kindly provided by Dr. Edward Thompson (University of Texas Medical Branch, Galveston, TX) and Dr. William Dalton (Lee Moffitt Cancer Center, Tampa, FL), respectively. MM and prostate cancer cells were cultured in RPMI-1640 containing 10% fetal bovine serum (FBS), 2 μM L-glutamine, 100 U/mL penicillin and 100 μg/mL streptomycin (Thermo Fisher). HEK293T cells were grown in Dulbecco's modified Eagle's medium supplemented with 10% fetal bovine serum (FBS), 2 μM L-glutamine, 100 U/mL penicillin and 100 μg/mL streptomycin (Thermo Fisher).

**Murine xenograft models of human MM**

Male NOD/Shi-scid, IL-2RγKOJic (NOG) mice were purchased from CLEA Japan Inc. Animal studies using MM.1S xenograft model were conducted according to Chiba University guidelines for the use of laboratory animals and approved by the Review Board for Animal Experiments of Chiba University (approval ID: 27-213). For single agent UNC1999 model: mice were inoculated subcutaneously in the right flank with $5 \times 10^6$ MM.1S cells in 100 μl RPMI-1640. After detection of tumors, mice were treated for 3 weeks with 25 mg/kg intraperitoneal UNC1999 twice a week (n=7). A vehicle control group (n=10) received intraperitoneal vehicle (5% DMSO in corn oil).

For the combination xenograft model, mice were inoculated subcutaneously in the right flank with $4 \times 10^6$ MM.1S cells in 100 μl RPMI-1640. After detection of tumors, mice were treated for 5 weeks with 15 mg/kg intraperitoneal UNC1999 3 days a week (n=14); 0.5 mg/kg subcutaneous bortezomib (Velcade®) in the left flank twice a week (n=13); or 15 mg/kg intraperitoneal UNC1999 3 days a week and 0.5 mg/kg subcutaneous bortezomib twice a week (n=13). A vehicle control group received intraperitoneal vehicle (5% DMSO in corn oil) and subcutaneous saline (n=14).

For all mice groups, tumor volume was calculated from caliper measurements every 3 - 4 days until day of first death in each group; mice were sacrificed when tumors reached 2,000 $cm^3$ or were ulcerated. Survival was evaluated from the first day of treatment until death.

**Reagents**

UNC1999 was produced at Icahn School of Medicine at Mount Sinai [9] and was diluted in DMSO to a stock of 10 mM for cell culture experiments. For in vivo experiments, UNC1999 was slowly dissolved in 5% DMSO in corn oil with vigorous vortex followed by

rotation to achieve a homogenous suspension of 60 or 100 mg/mL. GSK126 was purchased from CHEMIETEK and was diluted in DMSO to a stock of 20 mM. Bortezomib and carfilzomib for cell culture experiments were obtained from Selleck Chemicals and were diluted in DMSO to stocks of 100 μM. Bortezomib was purchased from Janssen Pharmaceutical KK for in vivo experiments and was diluted in normal saline to a 1mg/mL stock. MG132 was obtained from Cayman Chemical and was diluted in DMSO to a stock of 10 mM.

HLM006474 [25] was purchased from Sigma-Aldrich and was diluted in DMSO to a stock of 10 mM.

**RNA-seq library construction and sequencing analysis**

Total RNA was purified from 2 x $10^6$ MM.1S cells using the RNeasy plus Micro Kit (QIAGEN). RNA concentration and integrity were verified using Agilent 2100 Bioanalyzer (Santa Clara, CA, USA). Amplification, construction of the libraries and sequencing were performed as previously described [26]. TopHat (version 1.3.2; with default parameters) was used to align to the human reference genome (hg19 from University of California, Santa Cruz Genome Browser; http://genome.ucsc.edu/). Then, gene expression values were calculated as reads per kilobase of exon unit per million mapped reads (RPKM) using cufflinks (version 2.0.2).

**ChIP-sequencing**

ChIP was performed using a previously described protocol [26], with the following modifications: MM.1S cells were digested with micrococcal nuclease (MNase) (Worthington). DNA libraries were prepared from 3 ng immunoprecipitated DNA and input samples using a ThruPLEX DNA-seq Kit (Rubicon Genomics) according to the manufacturer's instructions.

**Accession numbers**

RNA- and ChIP-sequencing data obtained in this study were deposited in DNA Data Bank of Japan (DDBJ) (DDBJ, accession number DRA004880).

**Statistical analysis**

Statistical significance of difference was measured by unpaired 2-tailed Student's t test or Welch's test when the variance was judged as significantly different. P values less than 0.05 were considered significant, using StatMate III version 3.18. Survival was assessed using Kaplan–Meier curves (Graph Pad Prism, version 4) and log-rank analysis using StatMate III version 3.18. Kruskal-Wallis test was used when more than two groups needed to be compared. Pearson's product-moment correlation was utilized to determine the presence of correlation. The combined effect of UNC1999 with bortezomib or carfilzomib was analyzed by isobologram analysis using the Compu-Syn software program (ComboSyn, Inc.) [27].

**Immunoblot analysis**

Whole-cell lysates were prepared by lysis in RIPA (50 mM Tris, pH 8.0, 150 mM NaCl, 1mM EDTA, pH 8.0,1% TritonX-100, 0.1% sodium deoxycholate and 0.1% SDS), PML (20 mM sodium phosphate, pH 7.0, 300 mM NaCl, 5 mM EDTA and 0.1% NP40) buffers supplemented with protease inhibitor cocktail (Roche) or SDS-sample buffer (25 mM Tris, pH 6.8, 1% SDS, 5% glycerol, 0.05% bromophenol blue and 1% β-mercaptoethanol). Lysates were then sonicated (Bioruptor, COSMO BIO CO.) prior to SDS-PAGE. Immunoblotting was performed according to standard procedures. Membranes were probed with the indicated antibodies to: H3 (Abcam, ab1791), H3K27me3 (Millipore, 07449), EZH2 (clone DC9, Cell Signaling, 5246), EZH1 (Abcam, ab86128), caspase-3 (Cell Sigaling, 9662),

caspase-8 (clone 1C12, Cell Signaling, 9746), caspase-9 (Cell Signaling, 9502), PARP (Cell Signaling, 9542), GAPDH (clone 14C10, Cell Signaling, 2118), E2F1 (clone C20, Santa Cruz, sc-193), phospho-RB (clone Ser 780, Santa Cruz, sc-12901), p21 (clone 12D1, Cell Signaling, 2947), p27 (clone C-19, Santa Cruz, sc-528), α-tubulin (Calbiochem, CP06), Nur77 (D63C5, Cell Signaling, 3960), and MYC (clone N-262, Santa Cruz, sc-764). HRP-conjugated secondary antibodies were purchased from Amersham ECL. Immobilon Western Chemiluminescent substrates (EMD Millipore) were used for immunoblot detection. Sequential reprobing of the membranes was performed after stripping of primary and secondary antibodies using 62.5mM Tris, pH 6.8, 2% SDS and 0.7% β-mercaptoethanol. Protein expression was quantified using Image Lab software (BioRad).

**Assay of apoptosis**

MM cell lines were plated at 1 x $10^6$ cells per well of a six-well plate and treated with or without UNC1999 (5μM) for 48 hours with bortezomib (5 nM) in the last 24 hours. Cells were harvested, washed with phosphate-buffered saline (PBS) and then stained with FITC Annexin V Apoptosis Detection Kit I (BD Pharmingen, 556547). Flow cytometry was performed on a BD FACS Canto II (BD Biosciences, San Jose, CA, USA) and analyzed using FlowJo software (Tree Star). Annexin V–positive and PI-negative cells were considered as early apoptotic, whereas positivity for both Annexin V and PI was regarded as indicative of late apoptosis.

**Assays of cytotoxicity**

Cell lines were dissociated, counted and plated in flat-bottom tissue culture 96-well plates (TPP). MM cell lines were plated at 8,000-20,000 cells per well and cultured for 72 hours with the indicated doses of UNC1999 or GSK126, and then the indicated doses of

bortezomib were added for the last 48 hours. For co-culture with BMSC medium experiments, MM cells were cultured in normal medium or conditioned medium derived from culture supernatant of BMSCs (BMSC medium) and then the cells were treated with UNC1999 and bortezomib as described above. Prostate cancer cell lines were plated at 4,000 cells per well and treated simultaneously with the indicated doses of UNC1999 or GSK126 and bortezomib for 72 hours. For MTS assay, CellTiter 96 AQueous One Solution (Promega) was added to the cells in the last four hours of the incubation period and absorbance was read on a plate reader (Synergy2, BioTeK, Winooski, VT, USA) to determine relative cell number in each well. Data were averaged for triplicates or quadruplicates and normalized to the untreated wells. Results are expressed as the percentage of untreated control. To calculate combination index, triplicate or quadruplicate data were averaged and input into CompuSyn software (ComboSyn) [27]. CI values of less than 1.0, equal to 1.0, and greater than 1.0 indicate synergism, additive effect, and antagonism, respectively.

**Quantitative RT-PCR**

Total RNA was isolated using TRI Reagent (Clinical Research Center) and cDNA was made using the ThermoScript RT-PCR system (Invitrogen) with an oligo-dT primer. Real-time quantitative PCR was performed in triplicate using FastStart Universal Probe Master (Roche Applied Science) and the indicated combinations of the Universal Probe Library (Roche Applied Science) on a StepOnePlus Real-Time PCR System (Applied Biosystems). The real-time PCR signals were examined in triplicates and normalized to those of *GAPDH* gene. The primers sequences and probes used are shown in table 6.

**Chromatin immunoprecipitation assays (ChIP)**

MM.1S cells incubated with bortezomib (5 nM) or DMSO for 24 hours were

crosslinked with 1% para-formaldehyde (PFA) and then sonicated (ultrasonic homogenizer, MICROTEC.CO). After centrifugation, the soluble chromatin fraction was recovered, pre-cleared with anti-rabbit IgG conjugated Dynabeads (Thermo Fisher), and then incubated with an anti-E2F1 (clone C20, Santa Cruz, sc-193) for 6 hours at 4˚C. On the following day, immunoprecipitates were thoroughly washed. A standard purification method was used to separate DNA from protein fragments. For ChIP assay, quantitative PCR was performed with Step One Plus real time PCR system using SYBR® Premix ExTaq II (Tli RNase Plus) from Takara. Primers for OCT4 (SIGMA-ALDRICH) were used as negative controls. Details of the primers used are shown in Table 7.

**Gene set enrichment analysis (GSEA)**

Gene set enrichment analysis was conducted with the software GSEA (http://www.broadinstitute.org/gsea) [28]. A pseudocount of 1 was added to the RPKM measure prior to GSEA.

**Vectors**

Lentiviral vectors (CS-H1-shRNA-EF-1α-EGFP) expressing short hairpin RNA (shRNA) that targets human *EZH2* (target sequence: sh-*EZH2*-1, 50-GGAAAGAACGGAAATCTTA -30; sh-*EZH2*-2, 50-GGATAGAGAATGTGGGTTT-30) and *luciferase* (*Luc*) were constructed [29]. Lentiviral vectors (CS-H1-shRNA-EF-1α-RFP) expressing short hairpin RNA (shRNA) that targets human *EZH1* (target sequence: sh-*EZH1*, 5'-GCGACTTCGACAACTTAAACG-3') were constructed. The *EZH2* overexpression construct was generated by subcloning murine *Ezh2* cDNA into CSII-EF-MCS-IRES2-Venus. *E2F1* overexpression retroviral vector (pMCs-E2F1-IG) was a kind gift from Dr. Yuji Furukawa at Jichi Medical School. *NR4A1* overexpression retroviral vector (MIG-R1-

NR4A1) was a kind gift from Dr. Akihiko Yoshimura at Keio University. Matched empty vectors were constructed. Recombinant lentiviruses and retroviruses were produced using established protocols [30].

**Luciferase assay**

HEK293T cells (8 x $10^4$ cells) were seeded in a 24 well plate and cultured for 24 hours. Cells were then transfected with 400 ng of the indicated expression vector (empty or *E2F1*) along with 100 ng of a reporter gene (pGL basic human *EZH2* promoter -1095bp, -442bp and -151bp to +48, respectively) and 20 pg of pRL-CMV, an expression vector of Renilla lucifesase, using FuGENE HD Transfection Reagent (Promega). 24 hours after transfection, the cells were subjected to luciferase assay using the Dual-luciferase Reporter System (Promega). Relative firefly Luciferase activities were calculated by normalizing transfection efficiency to Renilla Luciferase activities.

## Results

### UNC1999, a dual inhibitor of EZH2 and EZH1, inhibits the growth of MM cells

Confirming a previous report by siRNA method [14], knockdown of *EZH2* by shRNA using lentiviral vectors lead to growth inhibition in H929 myeloma cells following reduction in H3K27me3 levels with no significant change in H3K36me2 and H3K4me3 histone modifications (Fig. 1A-D), suggesting EZH2-dependency in MM. Interestingly, we found that *EZH1* knockdown by shRNA also induced growth inhibition in H929 cells, albeit less severe than that observed with *EZH2* knockdown (Fig. 1E). These data indicate that both EZH2 and EZH1 are essential for the growth of MM cells. To examine the impact of pharmacological inhibition of PRC2 activity on MM cells, we used UNC1999 [7,9] which exerts dual inhibition of the enzymatic activities of EZH2 and EZH1 ($IC_{50}$, EZH2 <10 nM; EZH1 45 nM). UNC1999 potently inhibited the growth of several MM cell lines including drug-resistant cells (DOX40) in dose- and time-dependent manners (Fig. 1F and G). Moreover, UNC1999 treatment resulted in a significant concentration- and time-dependent reduction in H3K27me3 level with little to no effect on EZH2 protein level nor on H3K36me2 and H3K4me3 histone modifications (Fig. 2A and B). Importantly, UNC1999 induced significant cytotoxicity in $CD138^+$ bone marrow plasma cells (BMPCs) of MM patients (Fig. 2C). When tested on mononuclear cells from healthy donors, UNC1999 caused minimal cytotoxicity at concentrations up to 5 μM. (Fig. 2D)

To determine the impact of dual inhibition of EZH2 and EZH1 on MM cells in vivo, we treated MM.1S xenograft-bearing NOG mice with 25 mg/kg of UNC1999 intraperitoneally (IP) twice a week for 3 weeks. The growth of xenografts treated with UNC1999 was significantly reduced compared with control ($p$<0.05 on day 22) (Fig. 2E). Taken together, these data show that PRC2 components EZH2 and EZH1 are valid therapeutic targets in MM both in vitro and in vivo.

**Bortezomib transcriptionally downregulates *EZH2* via E2F inactivation**

A recent study showed that bortezomib reduces EZH2 protein [31], which prompted us to thoroughly investigate the impact of proteasome inhibitors on EZH2. Interestingly, bortezomib downregulated not only EZH2 protein but also its mRNA in MM cells in dose- and time-dependent manners (Fig. 3A-C). This was also observed using two other proteasome inhibitors, namely carfilzomib and MG132 (Fig. 3D-G). However, EZH2 protein in bortezomib-resistant cell line KMS11/BTZ was not downregulated by bortezomib compared to the parental cell line KMS11 (Fig. 3H and I), suggesting a possible role of EZH2 downregulation in bortezomib-induced cytotoxity.

To dissect the mechanism underlying the repression of EZH2 by bortezomib, we focused on RB-E2F pathway as EZH2 is a downstream target of E2F transcription factors [32]. We found that bortezomib downregulated *E2F1* and *E2F2* mRNA as well as E2F1 and phosphorylated RB proteins, suggesting that RB-E2F pathway was abrogated by bortezomib (Fig. 4A and B). It is known that bortezomib blocks the degradation of cyclin-dependent kinase inhibitors (CDKIs), resulting in their accumulation and subsequent induction of cell-cycle arrest [33]. Our data confirmed that CDKIs p21 and p27 were stabilized by bortezomib (Fig. 4C). We next confirmed the previous finding that E2F1 transactivates *EZH2* promoter [32] using luciferase reporter assay (Fig. 4D). Moreover, ChIP assays in MM.1S cells revealed that bortezomib significantly inhibited the binding of E2F1 to *EZH2* promoter (Fig. 4E). Notably, overexpression of *E2F1* lead to remarkable upregulation of *EZH2* in H929 cells (Fig. 4F). In addition, E2F inhibitor, HLM006474, significantly downregulated *EZH2* mRNA confirming that *EZH2* repression by bortezomib is mediated through E2F1 (Fig. 4G) These results indicate that bortezomib treatment leads to accumulation of CDKIs p21 and p27 with subsequent reduction of RB phosphorylation, resulting in inactivation of E2F family, which in turn downregulates *EZH2* in MM cells.

**UNC1999 enhances cytotoxicity induced by proteasome inhibitors**

To determine if EZH2 plays a role in the response and/or resistance to bortezomib, we next studied the gene expression of pre-treatment samples from MM patients enrolled on the APEX 039 clinical study who received bortezomib treatment [34]. Our analysis using this database revealed that patients with higher levels of *EZH2* expression have poorer response to bortezomib (Fig. 5A and B). Furthermore, *EZH2* overexpression using a lentiviral vector in RPMI8226 and H929 cells conferred resistance to bortezomib compared to cells transduced with an empty vector (Fig. 6A and B). Interestingly, RPMI8226 cells transduced with *EZH2* lentivirus vector gained growth advantage over those transduced with the empty vector (Fig. 6C). To unveil the molecular mechanism underlying EZH2-dependent bortezomib resistance, we performed RNA sequencing of RPMI8226 cells transduced with *EZH2*-overexpressing or empty vectors. Analysis of RNA-seq data showed that MYC targets, ribosome, oxidative phosphorylation and G1-S transition gene sets were strongly enriched in RPMI8226 cells overexpressing *EZH2* (Fig. 6D and Table 5). These aggressive features of MM cells overexpressing *EZH2* might be associated with acquired resistance to bortezomib. Importantly, UNC1999 treatment overcame this resistance to bortezomib conferred by *EZH2* (Fig. 6A and B), clearly supporting the rationale of the combination of UNC1999 and proteasome inhibitors such as bortezomib in MM cells.

We found that UNC1999 enhanced the cytotoxicity induced by bortezomib or carfilzomib in MM cell lines with significant suppression of EZH2 and H3K27me3 (Fig. 7A-F), even in the presence of conditioned media derived from bone marrow stromal cells (BMSCs) to mimic the microenvironment of the bone marrow (Fig. 8A). Moreover, the enhanced cytotoxicity was similarly observed in DOX40 and KMS11/BTZ cell lines which are resistant to doxorubicin and bortezomib, respectively (Fig. 7D and E). These results were validated using the combination index (CI) [27] which confirmed the synergism between

UNC1999 and bortezomib or carfilzomib (CI<1.0) (Fig. 7A-D and Table 1A-E). In addition, UNC1999 enhanced the cytotoxicity induced by bortezomib in $CD138^+$ BMPCs derived from MM patients (Fig. 8B). In contrast, minimal cytotoxicity was observed in peripheral blood mononuclear cells isolated from healthy donors treated with the combination of UNC1999 and bortezomib (Fig. 8C).

To elucidate the mechanisms of the cytotoxicity induced by this combination, we conducted flow cytometric analysis using Annexin V staining and found that the percentage of apoptotic cells had dramatically increased with the combination (Fig. 8D). We also confirmed the induction of apoptosis as evidenced by the cleavage of caspases-3, -8, -9 and PARP in MM cell lines treated with the combination (Fig. 8E). These results indicate that increased apoptosis is one mechanism through which UNC1999 enhances the cytotoxicity induced by bortezomib in MM cells.

We further investigated the efficacy of combined treatment of UNC1999 (15 mg/kg IP 3 times a week) and low-dose subcutaneous bortezomib (0.5 mg/kg twice a week) in MM.1S xenograft model in NOG mice for 5 weeks. Notably, the combination significantly reduced the size of the tumors as compared to either single agent (Fig. 9A). Importantly, the combination treatment significantly prolonged the survival of mice without overt weight loss (Fig. 9B and C). These results illustrate that UNC1999 enhances bortezomib-induced cytotoxicity of myeloma cells not only in vitro but also in vivo.

**Genome-wide analyses unveil the UNC1999-target genes in MM cells**

To explore the genome-wide effects and target genes of UNC1999 and the combination with bortezomib, we performed RNA sequencing (RNA-seq) of MM.1S cells treated with 5 μmol/L of UNC1999 for 72 hours, 5 nmol/L of bortezomib for 48 hours, or the combination of both agents (UNC1999 for 72 hours with bortezomib in the last 48 hours)

versus DMSO-treated cells, and chromatin immunoprecipitation sequencing (ChIP-seq) for H3K27me3 of UNC1999 versus DMSO-treated control cells of the same experiment. We defined “PRC2 targets” as those with H3K27me3 enrichment greater than 2.0-fold over the input signal at the promoter region (transcriptional start site ± 2.0 kb) in MM.1S cells (Fig. 10A). ChIP-seq revealed that H3K27me3 levels at the promoters significantly decreased following UNC1999 treatment. Within PRC2 target genes, we defined genes that showed more than 2-fold reduction in H3K27me3 levels compared with DMSO-treated cells as "UNC1999 target genes" (Fig. 10A). Gene set enrichment analysis (GSEA) using our RNA-seq data confirmed that PRC2 target gene sets were significantly enriched in both UNC1999- and combination-treated cells (Fig. 10B and Table 2 and 3). Correspondingly, the expression of PRC2 target genes was significantly elevated in UNC1999- and combination-treated MM.1S cells as compared to DMSO-treated control cells (Fig. 10C). Among the PRC2 target genes, we selected 74 genes with significantly enhanced expression (>1.5-fold UNC1999/Control) and remarkable reduction of H3K27me3 (≥2-fold) upon UNC1999 treatment (Fig. 10D and Table 4) as major UNC1999 target genes in MM.1S cells. These genes included nuclear receptor transcription factor, *NR4A1* (also known as *NUR77*), cell growth-, differentiation-, and apoptosis-related, *EGR1*, the cell cycle regulator, *CDKN1C (also known as p57, KIP2)*, and component of NF-κB, *LTB*. While *LTB* and *EGR1* are novel tumor suppressor candidates in MM [35,36], *CDKN1C* is known as a direct target of EZH2 [37] and a tumor suppressor with prognostic value in several cancers [38].

**UNC1999-induced upregulation of *NR4A1* suppresses *MYC* with resultant MM growth suppression**

Among the major UNC1999 target genes, we focused on *NR4A1*. The upregulation of *NR4A1* by UNC1999 was confirmed by RT-PCR (Fig. 10E), and the other NR4A family

genes *NR4A2* (also known as *NURR1*) and *NR4A3* (also known as *NOR1*) were also upregulated by UNC1999 (Fig. 10F and G). Reduction of H3K27me3 levels at the *NR4A1* promoter was confirmed by a ChIP assay (Fig. 10H). Remarkably, overexpression of *NR4A1* lead to growth arrest in MM cells (Fig. 10I), indicating a tumor-suppressive function of NR4A1 in MM as previously implied [39]. *MYC* (also known as *c-Myc*), one of the key genes in MM pathogenesis, is reportedly a direct target of NR4As which repress its expression, and NR4A1 specifically occupies *MYC* promoter region upon NR4A expression [40]. Importantly, we found that overexpression of *NR4A1* resulted in remarkable downregulation of *MYC* (Fig. 11A). Moreover, *MYC* mRNA and its protein were suppressed by UNC1999 (Fig. 11B and C) leading to repression of MYC target gene sets (Fig. 11D). This suppression of *MYC* was further enhanced by the combination treatment (Fig. 11B-D). To determine the clinical relevance of these findings, we examined the gene expression of *NR4A1* and *MYC* in MM samples of patients treated with bortezomib in the APEX 039 clinical study [34]. Responsive (R) patients to bortezomib tended to have higher levels of *NR4A1* than nonresponsive (NR) ones. In addition, *MYC* expression was significantly higher in nonresponsive than responsive patients, suggesting an association between bortezomib-resistance and *MYC*. (Fig. 11E). Consistent with our in vitro data, *EZH2* levels were negatively correlated with *NR4A1*, albeit not statistically significant, and *MYC* and *NR4A1* showed a significant inverse correlation (Fig. 11F). Taken together, these data indicate that *NR4A1* is one of the target genes of UNC1999 in MM and triggers *MYC* downregulation which is enhanced by the combination with bortezomib.

**UNC1999 and bortezomib cooperatively suppress PRC2 function**

Although bortezomib downregulated *EZH2*, it did not significantly enrich the polycomb gene set in GSEA of our RNA-seq data (NES 0.635, FDR q-value 1.0, p value-1.0).

Immunoblotting and RT-PCR confirmed the downregulation of EZH2 following bortezomib treatment; in contrast, EZH1, the homolog of EZH2, was maintained and the global H3K27me3 levels were not reduced at all (Fig. 12A and B). Correspondingly, the sensitivity of H929 cells to bortezomib was only slightly enhanced following shRNA knockdown of *EZH2* (Fig. 12C). Therefore, we examined the effect of simultaneous knockdown of *EZH2* and *EZH1* on myeloma cells. While *EZH1* knockdown alone impaired the growth of MM cells, double knockdown of *EZH2* and *EZH1* induced rapid cell death of H929 cells (Fig. 1E). These results indicate that dual inhibition of *EZH2* and *EZH1* is required to obtain maximal anti-myeloma effect. Next, we performed side by side experiments to compare the dual inhibition of EZH2 and EZH1 with the specific inhibition of EZH2 as a partner of bortezomib, using UNC1999 and GSK126 ($IC_{50}$, EZH2 9.9 nM; EZH1 680 nM) [41], respectively. We confirmed that GSK126, as a single agent, induces modest cytotoxicity in MM cell lines (Fig. 12D). UNC1999 exhibited much better combination effects than GSK126 in several cell lines as evidenced by combination index (Fig. 13A and B, and Table 1F and G). In agreement with these findings, the combination of bortezomib with UNC1999, but not GSK126, further reduced the levels of EZH2 and H3K27me3 (Fig. 13C). These results strongly suggest that co-inhibition of EZH2 and its homolog EZH1 is necessary to fully block the activity of PRC2 and effectively enhance the sensitivity of myeloma cells to bortezomib.

**UNC1999 demonstrates synergistic effects with bortezomib in prostate cancer**

EZH2 overexpression was found to be associated with disease progression in advanced prostate cancer [4]. We therefore studied the efficacy of the combination treatment of UNC1999 and bortezomib in prostate cancer cells. UNC1999 exhibited strong synergistic effects with bortezomib in LNCaP and DU145 cell lines (Fig. 14A and B and Table 1H and I). Noticeably, side by side experiments clearly showed that combining bortezomib with

UNC1999 demonstrated superior synergism than combining it with GSK126, the specific inhibitor of EZH2, emphasizing the importance of EZH1 inhibition in prostate cancer. (Fig. 14A and Table 1H). Moreover, we observed EZH2 downregulation by bortezomib also in LNCaP cells (Fig .14C). These results indicate that the strategy of dual inhibition of EZH2 and EZH1 in combination with proteasome inhibitors can be broadly applied to the treatment of PRC2-dependent tumors such as prostate cancer.

**Discussion**

In this study, we investigated the use of UNC1999, a dual inhibitor of EZH2 and EZH1, alone and in combination with proteasome inhibitors in MM both in vitro and in vivo, as well as in prostate cancer. Our analysis illustrated that MM patients with higher levels of *EZH2* expression tended to respond poorly to bortezomib. In line with these observations, *EZH2* overexpression by lentiviral vectors triggered bortezomib-resistance in MM cells which could be overcome by UNC1999. Most importantly, we have demonstrated potent synergistic cytotoxic effects between UNC1999 and proteasome inhibitors, and dissected the underlying mechanism of the synergy and its molecular signature in MM cells. Furthermore, we showed that bortezomib markedly downregulated *EZH2* transcription and its protein expression. Undeniably, the mechanisms of action of proteasome inhibitors are multi-faceted and include cell cycle arrest through the accumulation of CDK inhibitors [42]. Bortezomib stabilizes CDK inhibitors p21 and p27 leading to hypophosphorylation of RB, which in turn prevents E2F1 from binding to its target genes including the *E2F1* promoter, thereby repressing *E2F1* transcription [43]. Importantly, E2F1 is known to transactivate *EZH2* [32]. As expected, bortezomib treatment downregulated *E2F1* and decreased the binding of E2F1 to *EZH2* promoter.

We have previously shown that substantial amounts of H3K27me3 persist after deletion of *Ezh2* in a mouse model of myelodysplastic syndrome (MDS) [44]. This fact points out the role that EZH1 plays in maintaining reduced but notable levels of H3K27me3 in the absence of EZH2. In agreement, bortezomib-induced downregulation of EZH2 did not significantly impair PRC2 function. Importantly, we have demonstrated that the combination of UNC1999 and bortezomib resulted in superior cytotoxic effects than the combination of GSK126 and bortezomib in MM and prostate cancer cells. This could be explained by the fact that UNC1999 effectively blocks PRC2 activity by inhibiting both EZH2 and EZH1

while GSK126 only inhibits EZH2, allowing residual PRC2 activity through EZH1. PRC2 targets tumor suppressor genes and developmental regulator genes, thereby playing an oncogenic role in EZH2-dependent cancers [3]. As expected and previously reported in leukemic cells [7], transcriptional profiling showed de-repression of PRC2 target genes following UNC1999 treatment. Of note, we observed more significant de-repression of PRC2 target genes in the combination of UNC1999 and bortezomib, suggesting cooperative inhibition of PRC2 function by the combination. Taken together, these observations suggest that the dual inhibition of EZH2 and EZH1 sensitizes MM and prostate cancer cells to proteasome inhibition, and that epigenetic therapies targeting both EZH2 and EZH1 may be required to achieve a sustainable effect on PRC2-dependent cancers (Fig. 14D).

Among the most upregulated genes in UNC1999-treated cells was *NR4A1* and its upregulation was enhanced in cells treated with the combination of UNC1999 and bortezomib. Other members of the orphan nuclear receptor NR4A subgroup: *NR4A2* and *NR4A3* were also upregulated by UNC1999. *NR4As* are immediate early or stress response genes that can be induced by a vast number of stimuli such as growth factors, inflammatory cytokines, and mitogenic, and apoptotic signals [45]. Of note, reduction of *Nr4a1/3* gene expression leads to development of myelodysplastic and myeloproliferative diseases (MDS/MPN) [46], while targeted deletion of both genes induces lethal acute myeloid leukemia (AML) in mice [47]. A recent study showed that overexpression of *NR4A1* induced massive apoptotic cell death of aggressive lymphoma cell lines [48]. In MM, NR4A1-mimicking peptide induced Bcl-B dependent apoptosis in MM cells [39]. These findings define NR4A1 as a candidate tumor suppressor in MM. Using overexpression experiments, we confirmed the anti-oncogenic role of NR4A1 in MM. Significantly, *MYC* is reportedly a direct target of NR4As [40]. UNC1999 treatment profoundly suppressed *MYC* expression in MM cells. As previously reported [49], bortezomib alone also downregulated *MYC* probably due to reduced

E2F1, a transactivator of *MYC* [50], and enhanced UNC1999-induced suppression of *MYC* as evidenced by the marked suppression of *MYC*-related gene sets. Therefore, UNC1999 and bortezomib cooperatively repress the transcription of *MYC*, one of the most potent oncogenes in MM, resulting in a remarkable synergistic effect.

Other notable UNC1999 targets included two novel candidate tumor suppressor genes in MM; *LTB* and *EGR1*. *LTB,* a TNF family member [51] implicated in NF-κB pathway [52], was reportedly inactivated in MM patients [35]. *EGR1* encodes a protein that induces the expression of tumor suppressors such as *TP53* [53] and *PTEN* [54]. In MM, recurrent mutations of *EGR1* were reported [35]. In addition, low expression of *EGR1* strongly correlated with disease progression and knockdown of *EGR1* in MM cell lines conferred resistance to bortezomib [36]. *CDKN1C*, which encodes the cyclin-dependent kinase inhibitor p57 (also known as kip2), is another direct target of UNC1999. Inactivation of *CDKN1C* by aberrant methylation of its promoter has been reported in several types of cancer [55]. The detailed functions of these genes in the pathogenesis of MM remain to be unveiled in future studies.

In conclusion, our findings demonstrate that targeting both EZH2 and EZH1, alone and in combination with proteasome inhibitors could be a new therapeutic option for the treatment of PRC2-dependent cancers. Hopefully, this study will pave the way for clinical evaluation of this novel therapeutic approach.

**Acknowledgments**

I would like to express my deepest gratitude to my mentors: Dr. Atsushi Iwama and Dr. Naoya Mimura for their guidance and unceasing support. I appreciate the valuable contribution from Dr. Motohiko Oshima, Mr. Atsunori Saraya, Dr. Shuhei Koide, Dr. Yuko Kato, Dr. Kazumasa Aoyama, Dr. Yaeko Nakajima-Takagi, Dr. Changshan Wang, Dr. Tetsuhiro Chiba, Dr. Anqi Ma, Dr. Jian Jin, Dr. Tohru Iseki, and Dr. Chiaki Nakaseko. I also would like to thank Dr. Yuji Furukawa at Jichi Medical School and Dr. Akihiko Yoshimura at Keio University for providing us with *E2F1* and *NR4A1* expression vectors, respectively. I am profoundly grateful to Ms. Shorouq Mohammed Kamel Rizq for her critical review of the manuscript.

**Grant Support**

This work was supported in part by Grants-in-Aid for Scientific Research in Japan (#15H02544, #26860719, and #16K09839); Scientific Research on Innovative Areas "Stem Cell Aging and Disease" (#26115002) from MEXT, Japan; Next-generation Cancer Research Strategy Promotion project (16cm0106516h0001) from Japan Agency for Medical Research and Development (AMED); and grants from the Uehara Memorial Foundation; Yasuda Medical Foundation; Mochida Memorial Foundation; Tokyo Biochemical Research Foundation; and Kanae Foundation for the promotion of Medical Science.

**References**


1 Cao, R. *et al.* Role of histone H3 lysine 27 methylation in Polycomb-group silencing. *Science* **298**, 1039-1043 (2002).

2 Agger, K. *et al.* UTX and JMJD3 are histone H3K27 demethylases involved in HOX gene regulation and development. *Nature* **449**, 731-734 (2007).

3 Laugesen, A. & Helin, K. Chromatin repressive complexes in stem cells, development, and cancer. *Cell Stem Cell* **14**, 735-751 (2014).

4 Varambally, S. *et al.* The polycomb group protein EZH2 is involved in progression of prostate cancer. *Nature* **419**, 624-629 (2002).

5 Morin, R. D. *et al.* Somatic mutations altering EZH2 (Tyr641) in follicular and diffuse large B-cell lymphomas of germinal-center origin. *Nat Genet* **42**, 181-185 (2010).

6 Kim, K. H. & Roberts, C. W. M. Targeting EZH2 in cancer. *Nat Med* **22**, 128-134 (2016).

7 Xu, B. *et al.* Selective inhibition of EZH2 and EZH1 enzymatic activity by a small molecule suppresses MLL-rearranged leukemia. *Blood* **125**, 346-357 (2015).

8 Garapaty-Rao, S. *et al.* Identification of EZH2 and EZH1 small molecule inhibitors with selective impact on diffuse large B cell lymphoma cell growth. *Chem Biol* **20**, 1329-1339 (2013).

9 Konze, K. D. *et al.* An orally bioavailable chemical probe of the lysine methyltransferases EZH2 and EZH1. *ACS Chem Biol* **8**, 1324-1334 (2013).

10 Siegel, R. L., Miller, K. D. & Jemal, A. Cancer statistics, 2016. *CA Cancer J Clin* **66**, 7-30 (2016).

11 Dimopoulos, M. A., Richardson, P. G., Moreau, P. & Anderson, K. C. Current treatment landscape for relapsed and/or refractory multiple myeloma. *Nat Rev Clin Oncol* **12**, 42-54 (2015).

12 Kalushkova, A. *et al.* Polycomb target genes are silenced in multiple myeloma. *PLoS One* **5**, e11483 (2010).

13 van Haaften, G. *et al.* Somatic mutations of the histone H3K27 demethylase gene UTX in human cancer. *Nat Genet* **41**, 521-523 (2009).

14 Croonquist, P. A. & Van Ness, B. The polycomb group protein enhancer of zeste homolog 2 (EZH 2) is an oncogene that influences myeloma cell growth and the mutant ras phenotype. *Oncogene* **24**, 6269-6280 (2005).

15 Hernando, H. *et al.* EZH2 inhibition blocks multiple myeloma cell growth through upregulation of epithelial tumor suppressor genes. *Mol Cancer Ther* **15**, 287-298 (2016).

16 Neo, W. H., Lim, J. F., Grumont, R., Gerondakis, S. & Su, I. H. c-Rel regulates Ezh2 expression in activated lymphocytes and malignant lymphoid cells. *J Biol Chem* **289**, 31693-31707 (2014).

17 Agarwal, P. *et al.* Genome-wide profiling of histone H3 lysine 27 and lysine 4 trimethylation in multiple myeloma reveals the importance of Polycomb gene targeting and highlights EZH2 as a potential therapeutic target. *Oncotarget* **7**, 6809-6823 (2016).

18 Mimura, N., Hideshima, T. & Anderson, K. C. Novel therapeutic strategies for multiple myeloma. *Exp Hematol* **43**, 732-741 (2015).

19 Xu, K. *et al.* EZH2 oncogenic activity in castration-resistant prostate cancer cells is polycomb-independent. *Science* **338**, 1465-1469 (2012).

20 Milano, A., Iaffaioli, R. V. & Caponigro, F. The proteasome: a worthwhile target for the treatment of solid tumours? *European Journal of Cancer* **43**, 1125-1133 (2007).

21 Voutsadakis, I. A. & Papandreou, C. N. The ubiquitin-proteasome system in prostate cancer and its transition to castration resistance. *Urologic Oncology: Seminars and*

*Original Investigations* **30**, 752-761 (2012).

22 Mimura, N. *et al.* Blockade of XBP1 splicing by inhibition of IRE1alpha is a promising therapeutic option in multiple myeloma. *Blood* **119**, 5772-5781 (2012).

23 Mimura, N. *et al.* Selective and potent Akt inhibition triggers anti-myeloma activities and enhances fatal endoplasmic reticulum stress induced by proteasome inhibition. *Cancer Res* **74**, 4458-4469 (2014).

24 Ri, M. *et al.* Bortezomib-resistant myeloma cell lines: a role for mutated PSMB5 in preventing the accumulation of unfolded proteins and fatal ER stress. *Leukemia* **24**, 1506-1512 (2010).

25 Ma, Y. *et al.* A small-molecule E2F inhibitor blocks growth in a melanoma culture model. *Cancer Res* **68**, 6292-6299 (2008).

26 Mochizuki-Kashio, M. *et al.* Ezh2 loss in hematopoietic stem cells predisposes mice to develop heterogeneous malignancies in an Ezh1-dependent manner. *Blood* **126**, 1172-1183 (2015).

27 Chou, T.-C. & Talalay, P. Quantitative analysis of dose-effect relationships: the combined effects of multiple drugs or enzyme inhibitors. *Advances in Enzyme Regulation* **22**, 27-55 (1984).

28 Subramanian, A. *et al.* Gene set enrichment analysis: a knowledge-based approach for interpreting genome-wide expression profiles. *Proceedings of the National Academy of Sciences* **102**, 15545-15550 (2005).

29 Chiba, T. *et al.* 3-Deazaneplanocin A is a promising therapeutic agent for the eradication of tumor-initiating hepatocellular carcinoma cells. *International Journal of Cancer* **130**, 2557-2567 (2012).

30 Iwama, A. *et al.* Enhanced self-renewal of hematopoietic stem cells mediated by the polycomb gene product Bmi-1. *Immunity* **21**, 843-851 (2004).

31 Nara, M. *et al.* Bortezomib reduces the tumorigenicity of multiple myeloma via downregulation of upregulated targets in clonogenic side population cells. *PLoS One* **8**, e56954 (2013).

32 Bracken, A. P. *et al.* EZH2 is downstream of the pRB-E2F pathway, essential for proliferation and amplified in cancer. *The EMBO Journal* **22**, 5323-5335 (2003).

33 Albero, M. P. *et al.* Bortezomib decreases Rb phosphorylation and induces caspase-dependent apoptosis in Imatinib-sensitive and -resistant Bcr-Abl1-expressing cells. *Oncogene* **29**, 3276-3286 (2010).

34 Mulligan, G. *et al.* Gene expression profiling and correlation with outcome in clinical trials of the proteasome inhibitor bortezomib. *Blood* **109**, 3177-3188 (2007).

35 Bolli, N. *et al.* Heterogeneity of genomic evolution and mutational profiles in multiple myeloma. *Nat Commun* **5**, 2997 (2014).

36 Chen, L. *et al.* Identification of early growth response protein 1 (EGR-1) as a novel target for JUN-induced apoptosis in multiple myeloma. *Blood* **115**, 61-70 (2009).

37 Yang, X. *et al.* CDKN1C (p57) is a direct target of EZH2 and suppressed by multiple epigenetic mechanisms in breast cancer cells. *PLoS One* **4**, e5011 (2009).

38 Besson, A., Dowdy, S. F. & Roberts, J. M. CDK inhibitors: cell cycle regulators and beyond. *Developmental Cell* **14**, 159-169 (2008).

39 Luciano, F. *et al.* Nur77 converts phenotype of Bcl-B, an antiapoptotic protein expressed in plasma cells and myeloma. *Blood* **109**, 3849-3855 (2007).

40 Boudreaux, S. P., Ramirez-Herrick, A. M., Duren, R. P. & Conneely, O. M. Genome-wide profiling reveals transcriptional repression of MYC as a core component of NR4A tumor suppression in acute myeloid leukemia. *Oncogenesis* **1**, e19 (2012).

41 McCabe, M. T. *et al.* EZH2 inhibition as a therapeutic strategy for lymphoma with EZH2-activating mutations. *Nature* **492**, 108-112 (2012).

42 Rajkumar, S. V., Richardson, P. G., Hideshima, T. & Anderson, K. C. Proteasome inhibition as a novel therapeutic target in human cancer. *Journal of Clinical Oncology* **23**, 630-639 (2005).

43 Araki, K., Nakajima, Y., Eto, K. & Ikeda, M.-A. Distinct recruitment of E2F family members to specific E2F-binding sites mediates activation and repression of the E2F1 promoter. *Oncogene* **22**, 7632-7641 (2003).

44 Muto, T. *et al.* Concurrent loss of Ezh2 and Tet2 cooperates in the pathogenesis of myelodysplastic disorders. *The Journal of Experimental Medicine* **210**, 2627-2639 (2013).

45 Mohan, H. M. *et al.* Molecular pathways: the role of NR4A orphan nuclear receptors in cancer. *American Association for Cancer Research* **18**, 3223-3228 (2012).

46 Ramirez-Herrick, A. M., Mullican, S. E., Sheehan, A. M. & Conneely, O. M. Reduced NR4A gene dosage leads to mixed myelodysplastic/myeloproliferative neoplasms in mice. *Blood* **117**, 2681-2690 (2011).

47 Mullican, S. E. *et al.* Abrogation of nuclear receptors Nr4a3 andNr4a1 leads to development of acute myeloid leukemia. *Nat Med* **13**, 730-735 (2007).

48 Deutsch, A. J. A. *et al.* NR4A1-mediated apoptosis suppresses lymphomagenesis and is associated with a favorable cancer-specific survival in patients with aggressive B-cell lymphomas. *Blood* **123**, 2367-2377 (2014).

49 Zhao, W.-L. *et al.* PRDM1 is involved in chemoresistance of T-cell lymphoma and down-regulated by the proteasome inhibitor. *Blood* **111**, 3867-3871 (2008).

50 Hiebert, S. W., Lipp, M. & Nevins, J. R. E1A-dependent trans-activation of the human MYC promoter is mediated by the E2F factor. *Proceedings of the National Academy of Sciences* **86**, 3594-3598 (1989).

51 Browning, J. L. *et al.* Lymphotoxin β, a novel member of the TNF family that forms a

heteromeric complex with lymphotoxin on the cell surface. *Cell* **72**, 847-856 (1993).

52 Keats, J. J. *et al.* Promiscuous mutations activate the noncanonical NF-κB pathway in multiple myeloma. *Cancer Cell* **12**, 131-144 (2007).

53 Nair, P. *et al.* Early growth response-1-dependent apoptosis is mediated by p53. *Journal of Biological Chemistry* **272**, 20131-20138 (1997).

54 Virolle, T. *et al.* The Egr-1 transcription factor directly activates PTEN during irradiation-induced signalling. *Nat Cell Biol* **3**, 1124-1128 (2001).

55 Kikuchi, T. *et al.* Inactivation of p57KIP2 by regional promoter hypermethylation and histone deacetylation in human tumors. *Oncogene* **21**, 2741-2749 (2002).

**Figure legends**

**Figure 1. Pharmacological and lentiviral suppression of EZH2 and EZH1 in MM cell lines.**

H929 cells transduced with the indicated lentiviruses were selected by cell sorting for GFP expression, and subjected to: (A) Quantitative RT-PCR analysis of *EZH2* mRNA expression. Y-axis represents fold-change after normalization to *GAPDH*, and error bars represent SD of triplicates. (B) Immunoblot analysis for the indicated proteins. GAPDH and H3 served as loading controls. (C) Cell proliferation assay of H929 cells transduced with the indicated lentiviruses. Cell counting was performed using trypan blue on the indicated days of cultures. Data represent mean ± SD of triplicate cultures. (D) H929 cells transduced with the indicated lentiviruses were selected by cell sorting for GFP expression, and subjected to immunoblot analysis for the indicated proteins. H3 served as a loading control. (E) H929 cells transduced with the indicated lentiviruses were selected by cell sorting for GFP or RFP expression, and subjected to cell proliferation assay. Cell counting was performed using trypan blue on the indicated days of cultures. Y-axis represents log2. Red dashed line indicates that no live sh-EZH1+sh-EZH2-2 cells were detected on day 5. Data represent mean ± SD of triplicate cultures. (F) Cell proliferation assays of MM.1S, H929, RPMI8226 and DOX40 human myeloma cell lines treated with a range of concentrations of UNC1999 for 4 or 7 days. Cell counting was performed using trypan blue staining. Y-axis is presented as the mean cell count ± SD of triplicate cultures. (G) MTS assay showing viability of MM cell lines upon treatment with the indicated doses of UNC1999 (72 hours) relative to untreated control. Data represent mean ± SD of triplicates. *$P < 0.05$; **$P < 0.01$, ***$P < 0.001$; NS, not significant.

**Figure 2. UNC1999 blocks the trimethylation of H3K27 with subsequent inhibition of the growth of MM cells.**

(A) Immunoblot analyses for EZH2 and H3K27me3 after treatment of MM cells with a range of concentrations of UNC1999 for 72 hours (left panels) or 5 μmol/L of UNC1999 for the indicated times (right panels). H3 and GAPDH served as loading controls. (B) Immunoblot analyses for H3K36me2 and H3K4me3 in MM cells described in (A). H3 served as a loading control. (C) MTS assay showing viability of primary MM cells isolated from patients treated with 5 μmol/L of UNC1999 for 48 hours relative to untreated control. Data represent mean ± SD (n= 2~4). (D) MTS assay showing viability of peripheral blood mononuclear cells (PBMNCs) isolated from healthy donors upon treatment with the indicated doses of UNC1999 (48 hours) relative to untreated control. (E) In vivo analysis using murine xenograft model of human myeloma MM.1S cells inoculated into the flanks of NOG mice. When the tumor volume reached ~50 $mm^3$, UNC1999 was administered intraperitoneally (25 mg/kg), twice per week (n= 7) for 21 days. Tumor volume was calculated from caliper measurements and compared to vehicle-treated tumors (n= 10) at the indicated time points. Data represent mean ± SE. *$P < 0.05$; **$P < 0.01$.

**Figure 3. Proteasome inhibitors downregulate EZH2 in MM cell lines.**

(A) Immunoblot analysis for EZH2 after treatment of MM.1S cells with the indicated concentrations of bortezomib for 24 hours. GAPDH served as a loading control. (B-C) Quantitative RT-PCR analysis of *EZH2* mRNA expression in MM.1S cells treated with (B) the indicated doses of bortezomib for 8 hours or (C) 5 nmol/L of bortezomib for the indicated times. Y-axis represents fold-change after normalization to *GAPDH*, and error bars represent SD of triplicates. (D) Immunoblot analysis of EZH2 in MM.1S cells treated with the indicated doses of carfilzomib for 24 hours. GAPDH served as a loading control. (E) Quantitative RT-PCR analysis of *EZH2* mRNA expression in MM.1S cells treated with the indicated doses of carfilzomib for 12 hours. Y-axis represents fold-change after normalization

to *GAPDH*, and error bars represent SD of triplicates. (F) Immunoblot analysis of EZH2 in MM.1S cells treated with the indicated doses of MG132 for 24 hours. GAPDH served as a loading control. (G) Quantitative RT-PCR analysis of EZH2 mRNA expression in MM.1S cells treated with the indicated doses of MG132 for 12 hours. Y-axis represents fold-change after normalization to GAPDH, and error bars represent SD of triplicates. (H) MTS assay showing viability of KMS11 or KMS11/BTZ cells upon treatment with 10 nmol/L of bortezomib for 24 hours relative to untreated control. Data represent mean ± SD of triplicate cultures. (I) Immunoblot analysis of EZH2 in KMS11 or KMS11/BTZ cells treated with 10 nmol/L of bortezomib for 24 hours. GAPDH served as a loading control. *$P < 0.05$; **$P < 0.01$; ***$P < 0.001$.

**Figure 4. Bortezomib downregulates EZH2 via E2F inactivation.**

(A) Quantitative RT-PCR analysis of *E2F1* and *E2F2* mRNA expression in MM.1S cells treated with 5 nmol/L of bortezomib for 12 hours. Y-axis represents fold-change after normalization to *GAPDH*, and error bars represent SD of triplicates. (B-C) Immunoblot analyses for the indicated proteins in MM.1S cells upon (B) 24 hours or (C) 8 hours treatment with a range of concentrations of bortezomib. GAPDH and α-tubulin served as loading controls. (D) Luciferase reporter assays were performed in HEK293T cells with the indicated EZH2 promoter constructs. Reporters were co-transfected with either empty or E2F1 expression plasmids. Transfections were normalized by using a simultaneously delivered Renilla luciferase expression plasmid. Schematic representation of the reporters' constructs is depicted in upper panels. Data represent mean ± SD of triplicates. (E) Chromatin immunoprecipitation analysis for E2F1 occupancy on *EZH2* promoter in MM.1S cells treated with 5 nmol/L of bortezomib or DMSO for 24 hours. *OCT4* was used as a negative control. Values correspond to mean percentage of input enrichment ± SD of triplicate qPCR reactions

of a single replicate. Schematic representation of the location of the primer sets is depicted (upper panel). (F) Quantitative RT-PCR analysis of mRNA expression of *E2F1* and *EZH2* in H929 cells transduced with *E2F1* overexpressing or empty vectors. Y-axis represents fold-change after normalization to *GAPDH*, and error bars represent SD of triplicates. (G) Quantitative RT-PCR analysis of E2F1 and EZH2 mRNA expression in MM.1S cells treated with 5 μmol/L of HLM006474 for 12 hours. Y-axis represents fold-change after normalization to GAPDH, and error bars represent SD of triplicates. *$P < 0.05$; **$P < 0.01$; ***$P < 0.001$.

**Figure 5. MM patients with higher levels of EZH2 expression have poorer response to bortezomib.**

(A) Box-and-whisker plots showing the expression levels of EZH2 in pre-treatment samples from MM patients enrolled on the APEX 039 clinical study who received bortezomib treatment. Boxes represent 25 to 75 percentile ranges. Whiskers represent the most extreme data point which is no more than 1.5 times the interquartile range from the box. Red + represents mean value. Horizontal bars represent median. (B) EZH2 gene expression in MM patients in (A) is represented as a stacked bar chart. The range at the bottom of each bar represents the expression levels of EZH2 in the total cohort in(A). Bars are subdivided by patients' response to treatment, with segments proportional to percentage of patients. R, response; NR, nonresponse; CR, complete response; PR, partial response; MR, minimal response; NC, no change; PD, progressive disease. ***P < 0.001. (Kruskal-Wallis test).

**Figure 6. EZH2 overexpression in MM cells confers resistance to bortezomib through upregulation of gene sets related to MYC, cell cycle and metabolism.**

(A-B) MTS assays showing the viability of (A) RPMI8226 or (B) H929 cells transduced with

*EZH2*-overexpressing or empty vectors upon treatment with 5 µmol/L of UNC1999 (72 hours) and the indicated doses of bortezomib (last 48 hours) relative to untreated cells. Data represent mean ± SD of triplicates. Immunoblot analyses of the indicated proteins in *EZH2*-overexpressing or empty vector-transduced RPMI8226 or H929 cells are shown to the left of each graph. GAPDH and H3 served as loading controls. (C) Cell proliferation assay of RPMI8226 cells ($5 \times 10^4$ cells per well in 6-well plate) transduced with the indicated lentiviruses. Cell counting was performed using trypan blue at the indicated times. Y-axis is presented as the mean cell number ± SD of triplicates. (D) Representative gene sets significantly enriched in RPMI8226 cells transduced with EZH2-overexpressing versus empty vectors. NES, normalized enrichment score; q, FDR (false discovery rate) q value; p, p value. *P < 0.05; **P < 0.01; ***P < 0.001; NS, not significant.

**Figure 7. UNC1999 enhances the cytotoxicity induced by bortezomib in MM cell lines including resistant ones.**

(A-D) MTS assays showing viability of (A) H929, (B) MM.1S, (C) RPMI8226 and (D) DOX40 cells upon treatment with the indicated doses of UNC1999 (72 hours) in combination with the indicated doses of (A, C and D) bortezomib or (B) carfilzomib (last 48 hours), respectively, relative to untreated control. Data represent mean ± SD of triplicates. Calculation of combination index (CI) is shown to the right of each graph. (E) MTS assay showing viability of KMS11 or KMS11/BTZ cells upon treatment with 5 µmol/L of UNC1999 (72 hours) in combination with 40 nmol/L of bortezomib (last 48 hours) relative to untreated control. Data represent mean ± SD of triplicate cultures. (F) Immunoblot analyses for EZH2 and H3K27me3 after treatment of H929 (left panels) or MM.1S (right panels) cells with 5 µmol/L of UNC1999 for 72 hours and/or 5 nmol/L of bortezomib or carfilzomib for the last 12 or 24 hours, respectively. H3 and GAPDH served as loading controls.H3K27me3

amounts relative to total H3 are shown. *$P$ < 0.05; **$P$ < 0.01; ***$P$ < 0.001.

**Figure 8. UNC1999 augments bortezomib-induced cytotoxicity in vitro with significant induction of apoptosis but minimal effect on PBMNCs from healthy donors.**

(A) MTS assay showing the viability of MM.1S cells upon treatment with the indicated doses of UNC1999 (72 hours) in combination with the indicated doses of bortezomib (last 48 hours) in the presence of normal medium or BMSC medium, relative to untreated control in normal medium. Data represent mean ± SD of triplicates. (B) MTS assay showing the viability of primary MM cells isolated from patients treated simultaneously with 5 μmol/L of UNC1999 and the indicated doses of bortezomib for 48 hours relative to untreated control. Data represent mean ± SD (n= 3~4). (C) MTS assay showing the viability of PBMNCs isolated from healthy donors treated simultaneously with 5 μmol/L of UNC1999 and the indicated doses of bortezomib for 48 hours relative to untreated control. Data represent mean ± SD of triplicate cultures. (D) Propidium iodide (PI) and annexin V staining of MM.1S cells (upper panels) or H929 (lower panels) after incubation with or without UNC1999 (5 μmol/L) for 48 hours, or bortezomib (2.5 nmol/L) for 24 hours, or the combination (UNC1999 for 48 hours with bortezomib in the last 24 hours). Apoptotic cells were analyzed using flow cytometry. (E) Immnoblot analysis for the indicated proteins in MM.1S (left panels) and H929 (right panels) cells after treatment with 5 μmol/L of UNC1999 for 36 hours and/or 5 nmol/L of bortezomib for the last 12 hours. GAPDH served as a loading control. *P < 0.05; **P < 0.01; NS, not significant.

**Figure 9. UNC1999 enhances bortezomib-induced cytotoxicity in vivo without overt weight loss.**

(A) MM.1S cells were inoculated into the flanks of NOG mice. When the tumor volume

reached ~40 $mm^3$, mice were segregated into groups that received either vehicle (n= 14), 15 mg/kg of UNC1999 intraperitoneally three times per week (n= 14), 0.5 mg/kg of bortezomib subcutaneously twice per week (n= 13) or the combination of UNC1999 and bortezomib (n= 13) for 5 weeks. Tumor volume was calculated from caliper measurements at the indicated time points. Data represent mean ± SE. (B) Kaplan-Meier survival analysis of mice described in (A). Statistical significance of survival difference was determined by log-rank test. (C) Body weight of mice described in (A) and (B). Data represent mean ± SE. $*P < 0.05$; $**P < 0.01$; $***P < 0.001$.

**Figure 10. Identification of UNC1999-target genes in MM.1S cells.**

(A) A scatter plot showing the correlation of the fold enrichment values (ChIP/input) (TSS ± 2.0 kb) of H3K27me3 against the input signals of RefSeq genes between DMSO (control)- and UNC1999-treated MM.1S cells. Dotted diagonal line indicates 2-fold change. Blue box indicates PRC2 target genes (3,781 genes) with greater than 2-fold enrichment in H3K27me3 mark in the control. Red dots represent UNC1999 target genes with more than 2-fold reduction in H3K27me3 levels (2,167 genes). (B) Gene set enrichment plots for PRC2 target genes defined in (A) in MM.1S cells treated with UNC1999 alone (left) and combination (right) versus DMSO-treated control cells. NES, normalized enrichment score; q, FDR (false discovery rate) q value; p, p value (C) Box-and-whisker plots showing the expression changes of the top 1,000 PRC2 target genes defined in (A) in DMSO-, UNC1999-, bortezomib-, and combination- treated MM.1S cells. Boxes represent 25 to 75 percentile ranges. Vertical lines represent 10 to 90 percentile ranges. Horizontal bars represent median. (D) A scatter plot showing the correlation between the expression of genes and H3K27me3 levels in UNC1999- vs. DMSO-treated control MM.1S cells. Red dots indicate major UNC1999 target genes with significantly enhanced expression (>1.5-fold UNC1999/Control).

Representative genes are highlighted. (E) Quantitative RT-PCR analysis of *NR4A1* mRNA expression in MM.1S cells following treatment with 5 μmol/L of UNC1999 for 72 hours. Y-axis represents fold-change after normalization to *GAPDH*, and error bars represent SD of triplicates. (F) Quantitative RT-PCR analysis of mRNA expression of NR4A2 and NR4A3 in MM.1S cells treated with 5 μmol/L of UNC1999 for 72 hours. Y-axis represents fold-change after normalization to GAPDH, and error bars represent SD of triplicates. (G) Expression levels of NR4A1/2/3 in RPKM detected in RNA sequencing analysis of MM.1S cells treated with 5 μmol/L of UNC1999 for 72 hours versus DMSO-treated cells. (H) Chromatin immunoprecipitation analysis for H3K27me3 occupancy loss in promoter regions (TSS ± 2 kb) of *NR4A1* in MM.1S cells treated with 5 μmol/L of UNC1999 for 72 hours vs. DMSO-treated cells. Values correspond to mean percentage of input enrichment ± SD of triplicate qPCR reactions of a single replicate. (I) Cell proliferation assay of H929 cells (10,000 cells per well in 96-well plate) transduced with the indicated retroviruses for 48 hours prior to cell sorting for GFP expression. Cell counting was performed using trypan blue at the indicated times. Y-axis is presented as the mean cell number ± SD of quadruplicates. *P < 0.05; **P < 0.01; ***P < 0.001; NS, not significant.

**Figure 11. UNC1999-induced upregulation of *NR4A1* suppresses *MYC***

(A) Quantitative RT-PCR analysis of *MYC* mRNA expression in H929 cells transduced with *NR4A1*-overexpressing or empty vectors. Y-axis represents fold-change after normalization to *GAPDH*, and error bars represent SD of triplicates. (B) Quantitative RT-PCR analysis of *MYC* mRNA expression in MM.1S cells upon 72 hours of 5 μmol/L of UNC1999 and/or 5 nmol/L of bortezomib treatment for the last 12 hours. Y-axis represents fold-change after normalization to *GAPDH*, and error bars represent SD of triplicates. (C) Immunoblot analysis for the indicated proteins in MM.1S cells upon 72 hours of 5 μmol/L of UNC1999 and/or 5

nmol/L of bortezomib treatment for the last 12 hours. GAPDH was used as a loading control. (D) A representative MYC target gene set significantly enriched in MM.1S cells treated with UNC1999 alone (upper) and combination (lower) vs. DMSO-treated cells. NES, normalized enrichment score; q, FDR (false discovery rate) q value; p, p value. (E) Box-and-whisker plots showing the expression levels of NR4A1 (left) or MYC (right) in pre-treatment samples in responsive (R) vs. NR (nonresponsive) MM patients enrolled on the APEX 039 clinical study who received bortezomib treatment. Boxes represent 25 to 75 percentile ranges. Whiskers represent the most extreme data point which is no more than 1.5 times the interquartile range from the box. Red + represents mean value. Horizontal bars represent median. (F) Scatter plots showing the correlation between the expression of EZH2 and NR4A1 (left) or MYC and NR4A1 (right) in patients described in (E). Pearson's product-moment correlation was used to determine correlation. *$P$ < 0.05; **P<0.01; ***P<0.001; NS, not significant.

**Figure 12. Bortezomib alone is incapable of fully blocking PRC2 activity and the specific EZH2 inhibitor, GSK126, induces modest cytotoxicity in MM cells.**

(A) Immunoblot analysis for the indicated proteins in MM.1S cells after treatment with the indicated concentrations of bortezomib for 24 hours. GAPDH and H3 served as loading controls. (B) Quantitative RT-PCR analysis of mRNA expression of *EZH2* and *EZH1* in MM.1S cells treated with 5 nmol/L of bortezomib for 12 hours. Y-axis represents fold-change after normalization to *GAPDH*, and error bars represent SD of triplicates. (C) H929 cells transduced with the indicated lentiviruses were selected by cell sorting for GFP expression, and subjected to MTS assay. MTS assay showing viability of H929 cells upon treatment with the indicated doses of bortezomib (48 hours) relative to untreated control. Data represent mean ± SD of triplicates. (D) MTS assays showing viability of MM cell lines upon treatment

with the indicated doses of GSK126 (72 hours) relative to untreated control. Data represent mean ± SD of triplicates. ***P<0.001; NS, not significant.

**Figure 13. UNC1999 and bortezomib cooperatively suppress PRC2 function.**

(A) MTS assays performed side by side showing the viability of H929 cells upon treatment for 72 hours with the indicated doses of UNC1999 (left) or GSK126 (right) with the indicated doses of bortezomib in the last 48 hours relative to untreated control. Data represent mean ± SD of triplicate cultures. Combination index (CI) calculation is shown below each graph. (B) MTS assays performed side by side showing the viability of RPMI8226 cells upon treatment for 72 hours with the indicated doses of UNC1999 (left) or GSK126 (right) with the indicated doses of bortezomib in the last 48 hours relative to untreated control. Data represent mean ± SD of triplicate cultures. Combination index (CI) calculation is shown below each graph. (C) Immunoblot analysis for the indicated proteins in MM.1S cells upon 72 hours of 5 μmol/L of UNC1999 or GSK126 and/or 5 nmol/L of bortezomib treatment for the last 12 hours. GAPDH and H3 were used as loading controls. H3K27me3 amounts relative to total H3 are shown.

**Figure 14. UNC1999 enhances bortezomib-induced cytotoxicity in prostate cancer cells.**

(A) MTS assays performed side-by-side showing viability of LNCaP cells upon simultaneous treatment for 72 hours with the indicated doses of UNC1999 (left) or GSK126 (right) in combination with the indicated doses of bortezomib relative to untreated control. Data represent mean ± SD of triplicate cultures. Combination index (CI) calculation is shown below each graph. (B) MTS assay showing viability of DU145 cells upon simultaneous treatment for 72 hours with the indicated doses of UNC1999 and bortezomib relative to untreated control. Data represent mean ± SD of triplicate cultures. Combination index (CI)

calculation is shown to the right of the graph. (C) Immunoblot analysis for the indicated proteins in LNCaP cells after treatment with the indicated concentrations of bortezomib for 72 hours. GAPDH and H3 served as loading controls. (D) A proposed model for the synergistic activity of UNC1999 and bortezomib. Bortezomib downregulates EZH2 through stabilization of CDK inhibitors and inhibition of E2F1, while UNC1999 enhances the effect of bortezomib by suppressing both EZH2 and EZH1. This leads to de-repression of PRC2 target genes such as *NR4A1* resulting in inhibition of growth and proliferation of tumor cells.

# Figure 1

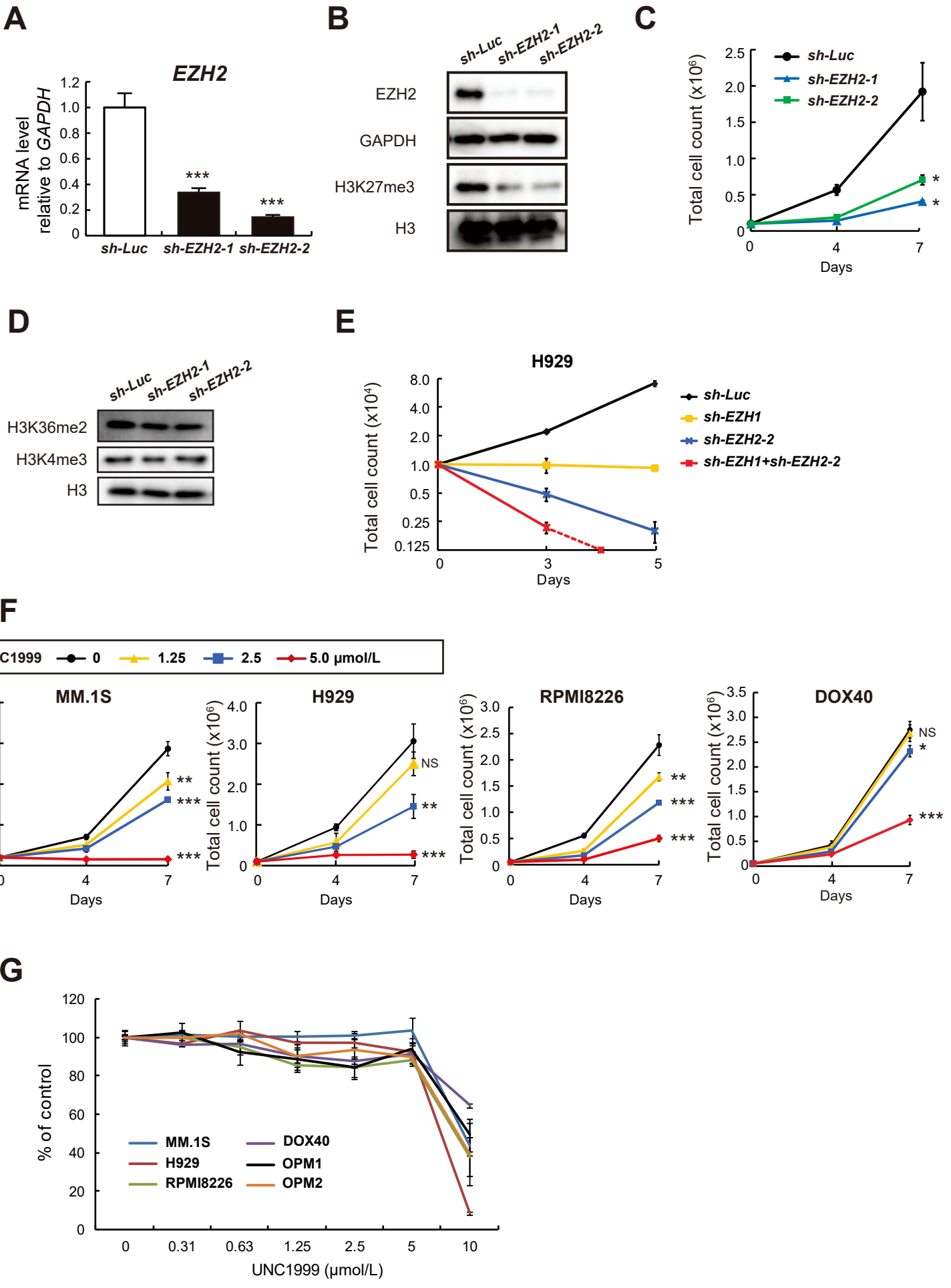
A
EZH2
mRNA level relative to GAPDH
1.2
1.0
0.8
0.6
0.4
0.2
0
***
***
sh-Luc
sh-EZH2-1
sh-EZH2-2
B
sh-Luc
sh-EZH2-1
sh-EZH2-2
EZH2
GAPDH
H3K27me3
H3
C
Total cell count (x10⁶)
2.5
2.0
1.5
1.0
0.5
0
sh-Luc
sh-EZH2-1
sh-EZH2-2
*
*
0
4
7
Days
D
sh-Luc
sh-EZH2-1
sh-EZH2-2
H3K36me2
H3K4me3
H3
E
H929
Total cell count (x10⁴)
8.0
4.0
2.0
1.0
0.5
0.25
0.125
0
3
5
Days
sh-Luc
sh-EZH1
sh-EZH2-2
sh-EZH1+sh-EZH2-2
F
UNC1999
0
1.25
2.5
5.0 μmol/L
MM.1S
H929
RPMI8226
DOX40
Total cell count (x10⁶)
Days
**
***
***
NS
**
***
**
***
NS
*
***
G
% of control
120
100
80
60
40
20
0
MM.1S
H929
RPMI8226
DOX40
OPM1
OPM2
0
0.31
0.63
1.25
2.5
5
10
UNC1999 (μmol/L)

# Figure 2

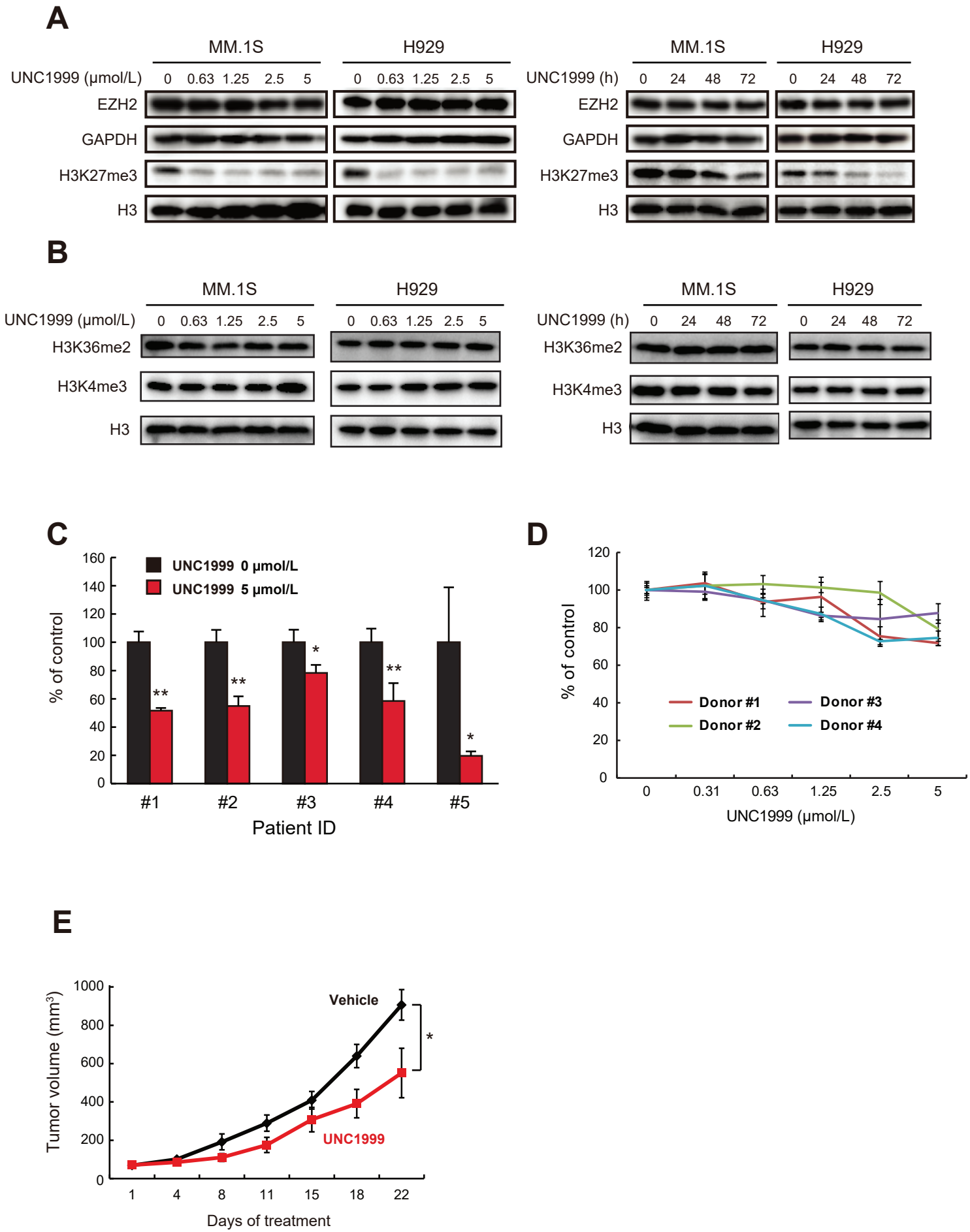
A
MM.1S
H929
UNC1999 (μmol/L)
0 0.63 1.25 2.5 5
EZH2
GAPDH
H3K27me3
H3
UNC1999 (h)
0 24 48 72
B
H3K36me2
H3K4me3
C
UNC1999 0 μmol/L
UNC1999 5 μmol/L
% of control
Patient ID
#1
#2
#3
#4
#5
D
Donor #1
Donor #2
Donor #3
Donor #4
UNC1999 (μmol/L)
E
Vehicle
UNC1999
Tumor volume (mm3)
Days of treatment

# Figure 3

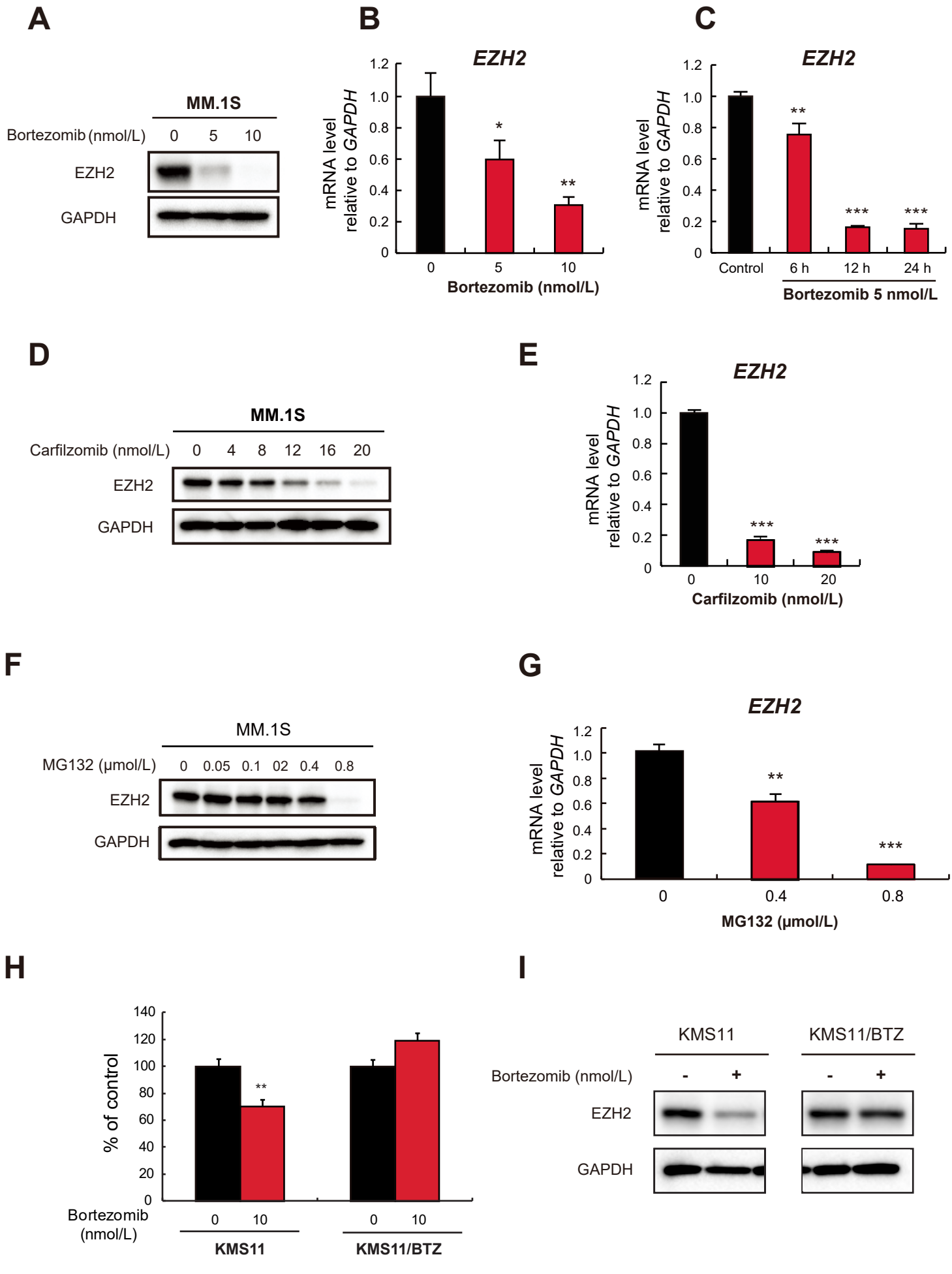
A
MM.1S
Bortezomib (nmol/L) 0 5 10
EZH2
GAPDH
B
EZH2
mRNA level relative to GAPDH
1.2
1.0
0.8
0.6
0.4
0.2
0
*
**
0 5 10
Bortezomib (nmol/L)
C
EZH2
mRNA level relative to GAPDH
**
***
***
Control 6 h 12 h 24 h
Bortezomib 5 nmol/L
D
MM.1S
Carfilzomib (nmol/L) 0 4 8 12 16 20
EZH2
GAPDH
E
EZH2
mRNA level relative to GAPDH
***
***
0 10 20
Carfilzomib (nmol/L)
F
MM.1S
MG132 (μmol/L) 0 0.05 0.1 02 0.4 0.8
EZH2
GAPDH
G
EZH2
mRNA level relative to GAPDH
**
***
0 0.4 0.8
MG132 (μmol/L)
H
% of control
140
120
100
80
60
40
20
0
**
Bortezomib (nmol/L)
0 10 0 10
KMS11
KMS11/BTZ
I
KMS11
KMS11/BTZ
Bortezomib (nmol/L) - + - +
EZH2
GAPDH

# Figure 4

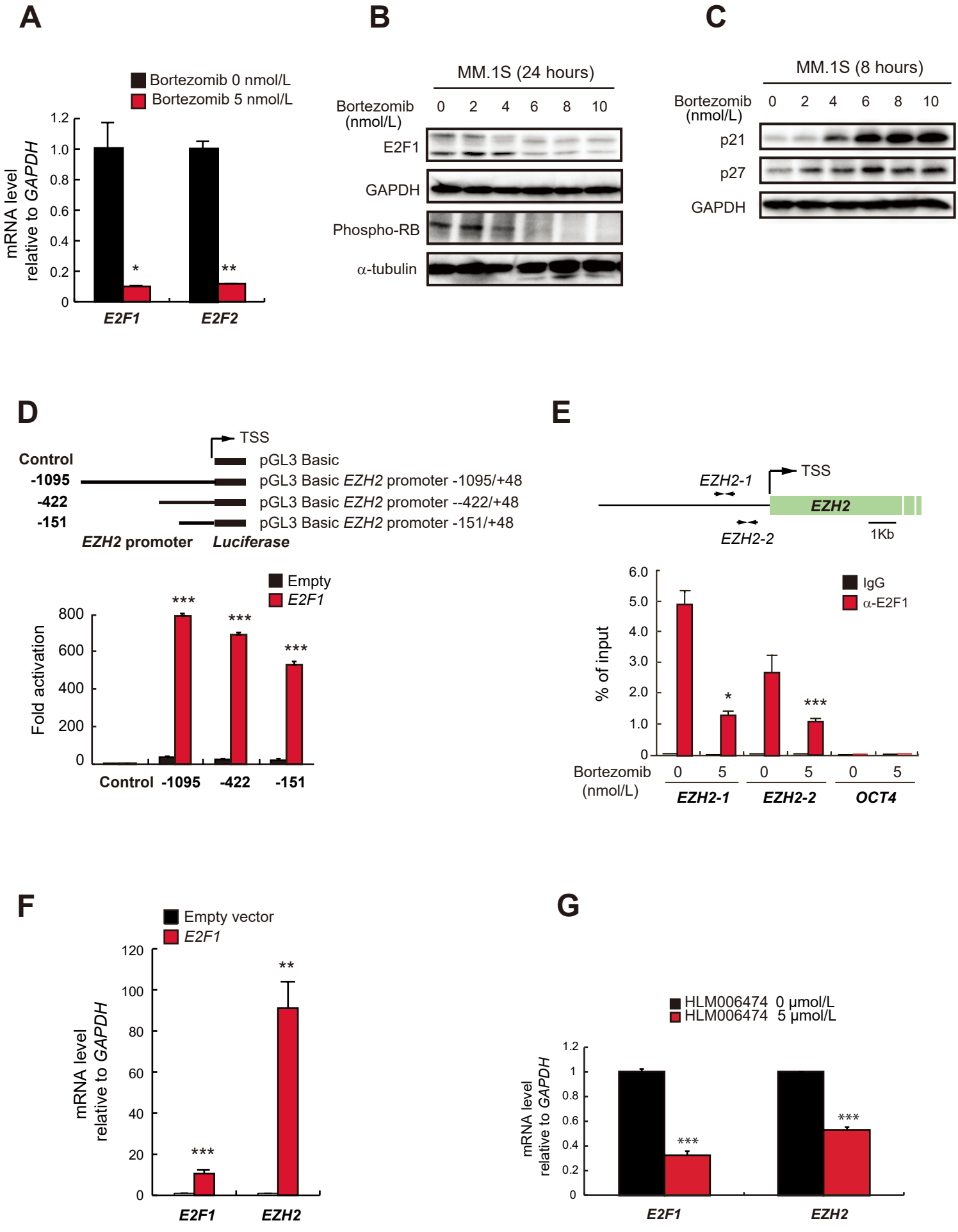
A
Bortezomib 0 nmol/L
Bortezomib 5 nmol/L
mRNA level relative to GAPDH
1.2
1.0
0.8
0.6
0.4
0.2
0
*
**
E2F1
E2F2
B
MM.1S (24 hours)
Bortezomib (nmol/L)
0 2 4 6 8 10
E2F1
GAPDH
Phospho-RB
α-tubulin
C
MM.1S (8 hours)
Bortezomib (nmol/L)
0 2 4 6 8 10
p21
p27
GAPDH
D
TSS
Control
pGL3 Basic
-1095
pGL3 Basic EZH2 promoter -1095/+48
-422
pGL3 Basic EZH2 promoter --422/+48
-151
pGL3 Basic EZH2 promoter -151/+48
EZH2 promoter
Luciferase
Empty
E2F1
Fold activation
800
600
400
200
0
***
***
***
Control
-1095
-422
-151
E
EZH2-1
TSS
EZH2
EZH2-2
1Kb
IgG
α-E2F1
% of input
6.0
5.0
4.0
3.0
2.0
1.0
0
*
***
Bortezomib (nmol/L)
0 5 0 5 0 5
EZH2-1
EZH2-2
OCT4
F
Empty vector
E2F1
mRNA level relative to GAPDH
120
100
80
60
40
20
0
**
***
E2F1
EZH2
G
HLM006474 0 μmol/L
HLM006474 5 μmol/L
mRNA level relative to GAPDH
1.2
1
0.8
0.6
0.4
0.2
0
***
***
E2F1
EZH2

# Figure 5

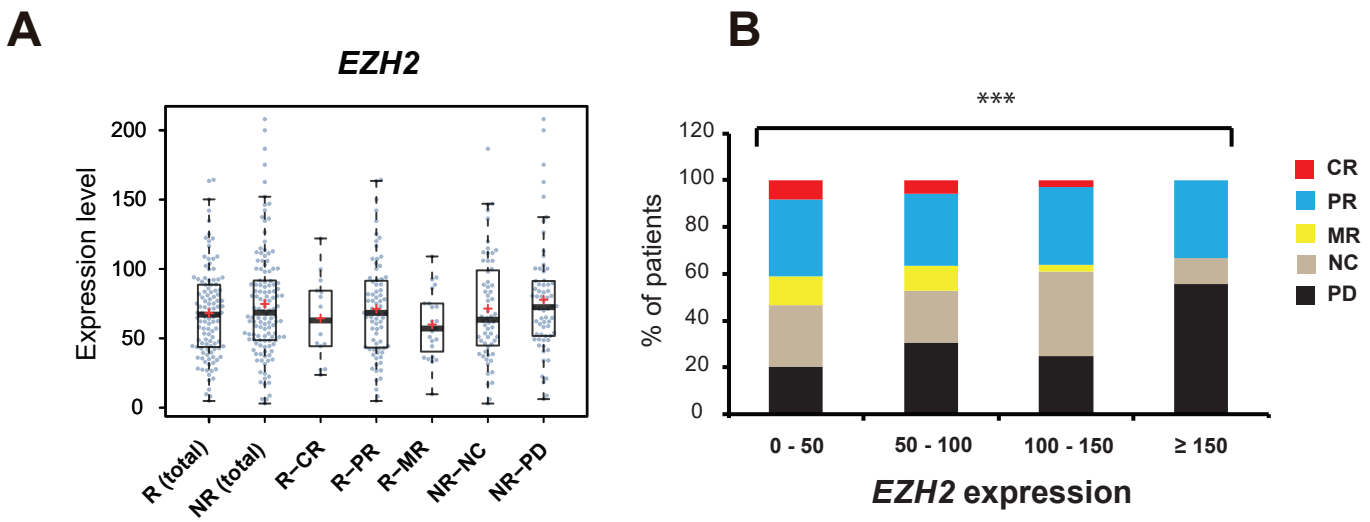
A
EZH2
Expression level
200
150
100
50
0
R (total)
NR (total)
R–CR
R–PR
R–MR
NR–NC
NR–PD
B
***
% of patients
120
100
80
60
40
20
0
0 - 50
50 - 100
100 - 150
≥ 150
EZH2 expression
CR
PR
MR
NC
PD

# Figure 6

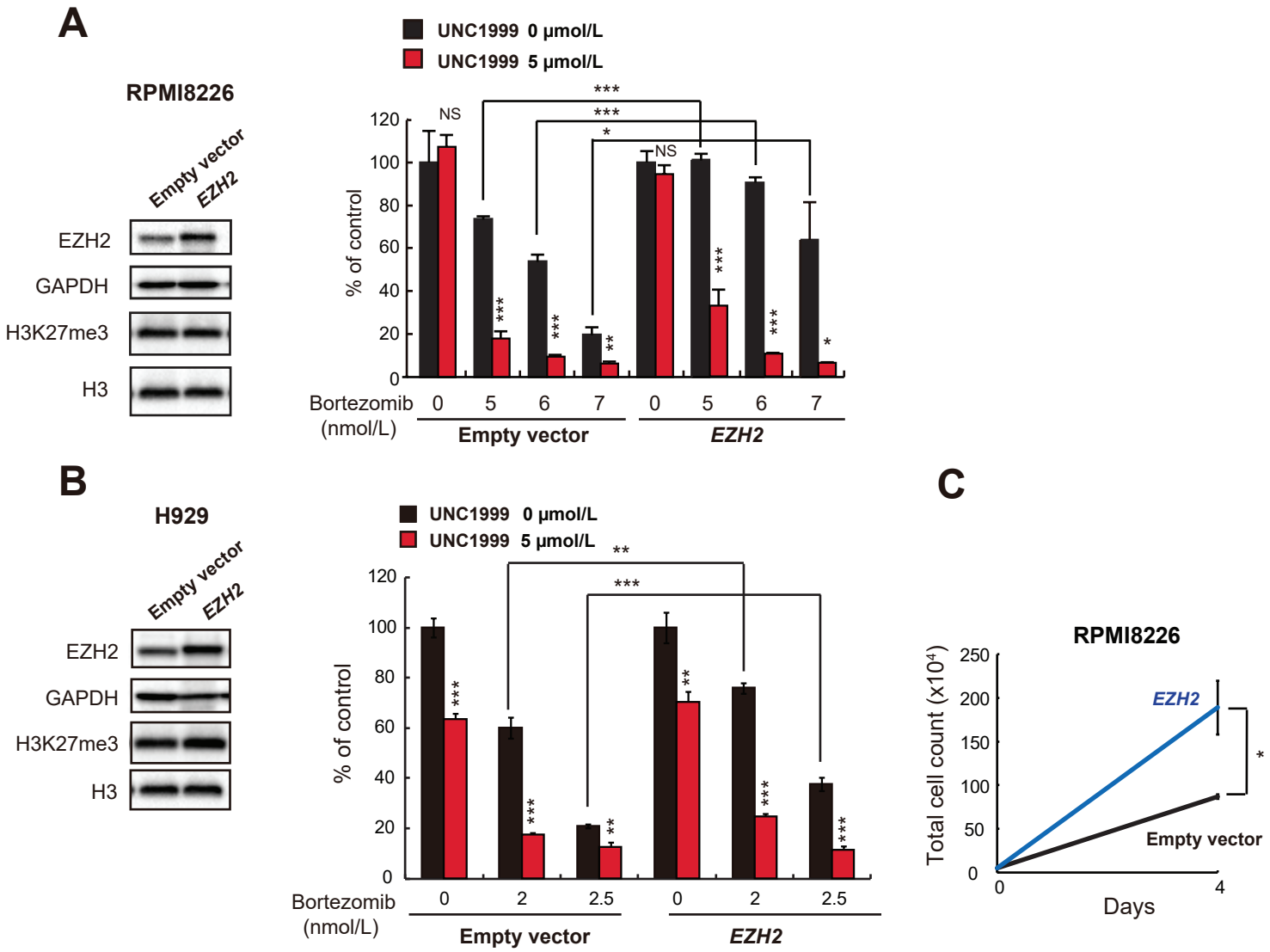
A
RPMI8226
Empty vector
EZH2
EZH2
GAPDH
H3K27me3
H3
UNC1999 0 μmol/L
UNC1999 5 μmol/L
% of control
Bortezomib (nmol/L)
Empty vector
EZH2
B
H929
C
RPMI8226
Total cell count (x10⁴)
Days
D
KEGG_RIBOSOME
NES 2.41
REACTOME_3_UTR_MEDIATED_TRANSLATIONAL_REGULATION
NES 2.40
REACTOME_METABOLISM_OF_RNA
NES 2.20
REACTOME_FORMATION_OF_THE_TERNARY_COMPLEX_AND_SUBSEQUENTLY_THE_43S_COMPLEX
NES 2.17
DANG_MYC_TARGETS_UP
NES 2.11
KEGG_OXIDATIVE_PHOSPHORYLATION
NES 2.11
SWEET_KRAS_ONCOGENIC_SIGNATURE
NES 1.98
REACTOME_MITOTIC_G1_G1_S_PHASES
NES 1.93

# Figure 7

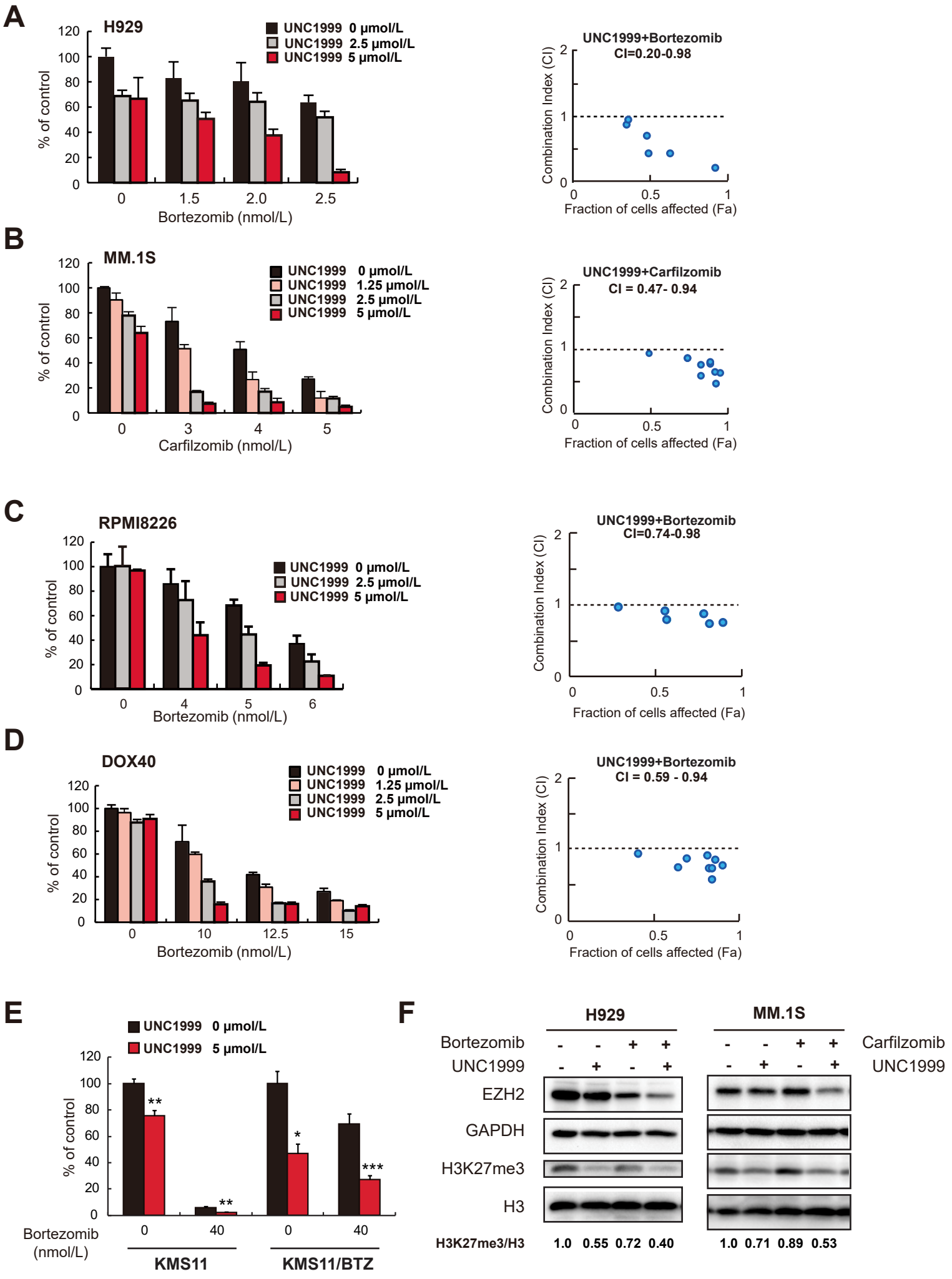
A
H929
UNC1999 0 μmol/L
UNC1999 2.5 μmol/L
UNC1999 5 μmol/L
% of control
Bortezomib (nmol/L)
UNC1999+Bortezomib
CI=0.20-0.98
Combination Index (CI)
Fraction of cells affected (Fa)
B
MM.1S
UNC1999 0 μmol/L
UNC1999 1.25 μmol/L
UNC1999 2.5 μmol/L
UNC1999 5 μmol/L
Carfilzomib (nmol/L)
UNC1999+Carfilzomib
CI = 0.47- 0.94
C
RPMI8226
UNC1999+Bortezomib
CI=0.74-0.98
D
DOX40
UNC1999+Bortezomib
CI = 0.59 - 0.94
E
KMS11
KMS11/BTZ
F
H929
MM.1S
Bortezomib
UNC1999
Carfilzomib
EZH2
GAPDH
H3K27me3
H3
H3K27me3/H3
1.0 0.55 0.72 0.40
1.0 0.71 0.89 0.53

# Figure 8

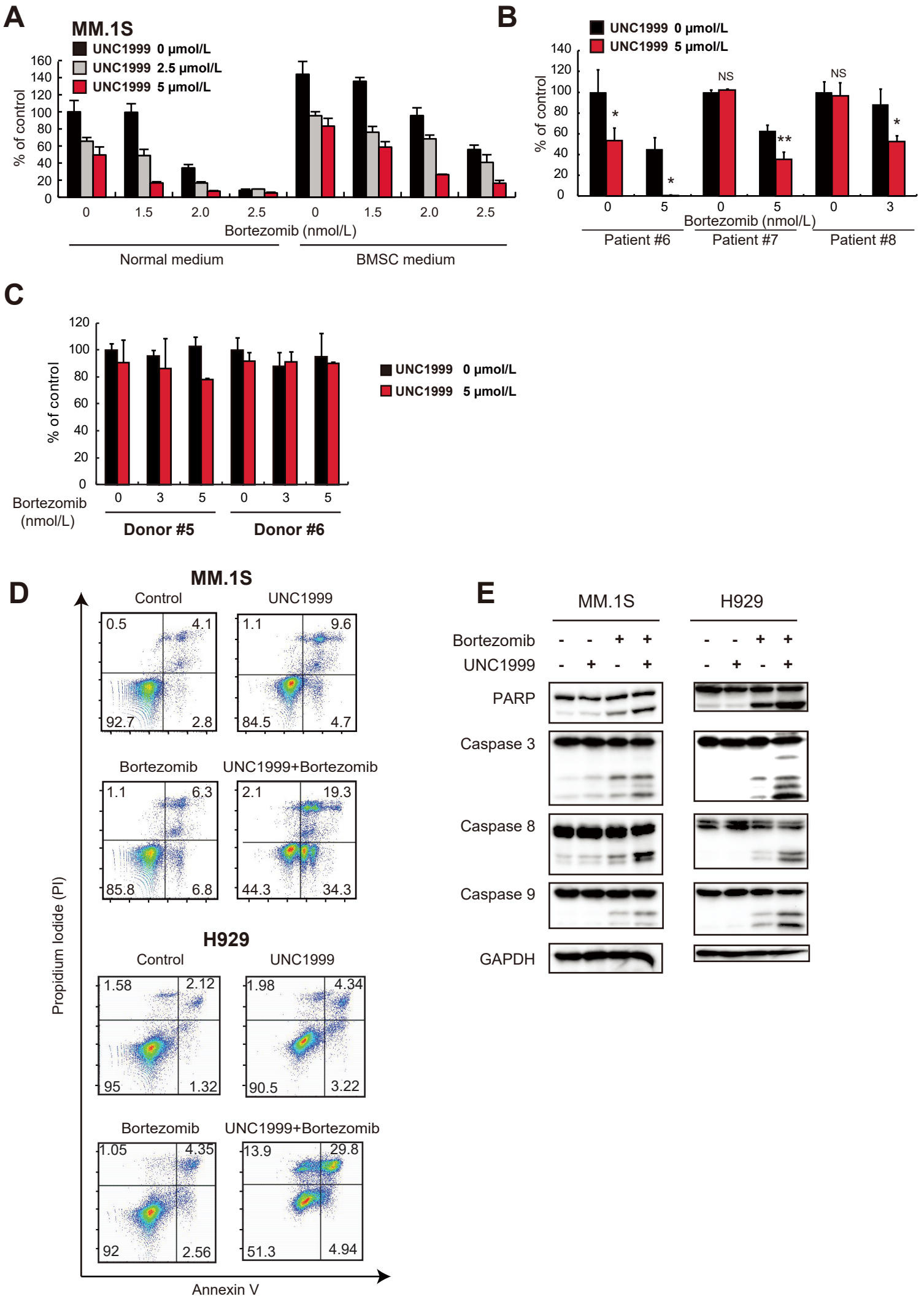
A
MM.1S
UNC1999 0 μmol/L
UNC1999 2.5 μmol/L
UNC1999 5 μmol/L
% of control
Bortezomib (nmol/L)
Normal medium
BMSC medium
B
UNC1999 0 μmol/L
UNC1999 5 μmol/L
% of control
NS
Bortezomib (nmol/L)
Patient #6
Patient #7
Patient #8
C
% of control
UNC1999 0 μmol/L
UNC1999 5 μmol/L
Bortezomib (nmol/L)
Donor #5
Donor #6
D
MM.1S
Control
UNC1999
Bortezomib
UNC1999+Bortezomib
H929
Propidium Iodide (PI)
Annexin V
E
MM.1S
H929
Bortezomib
UNC1999
PARP
Caspase 3
Caspase 8
Caspase 9
GAPDH

# Figure 9

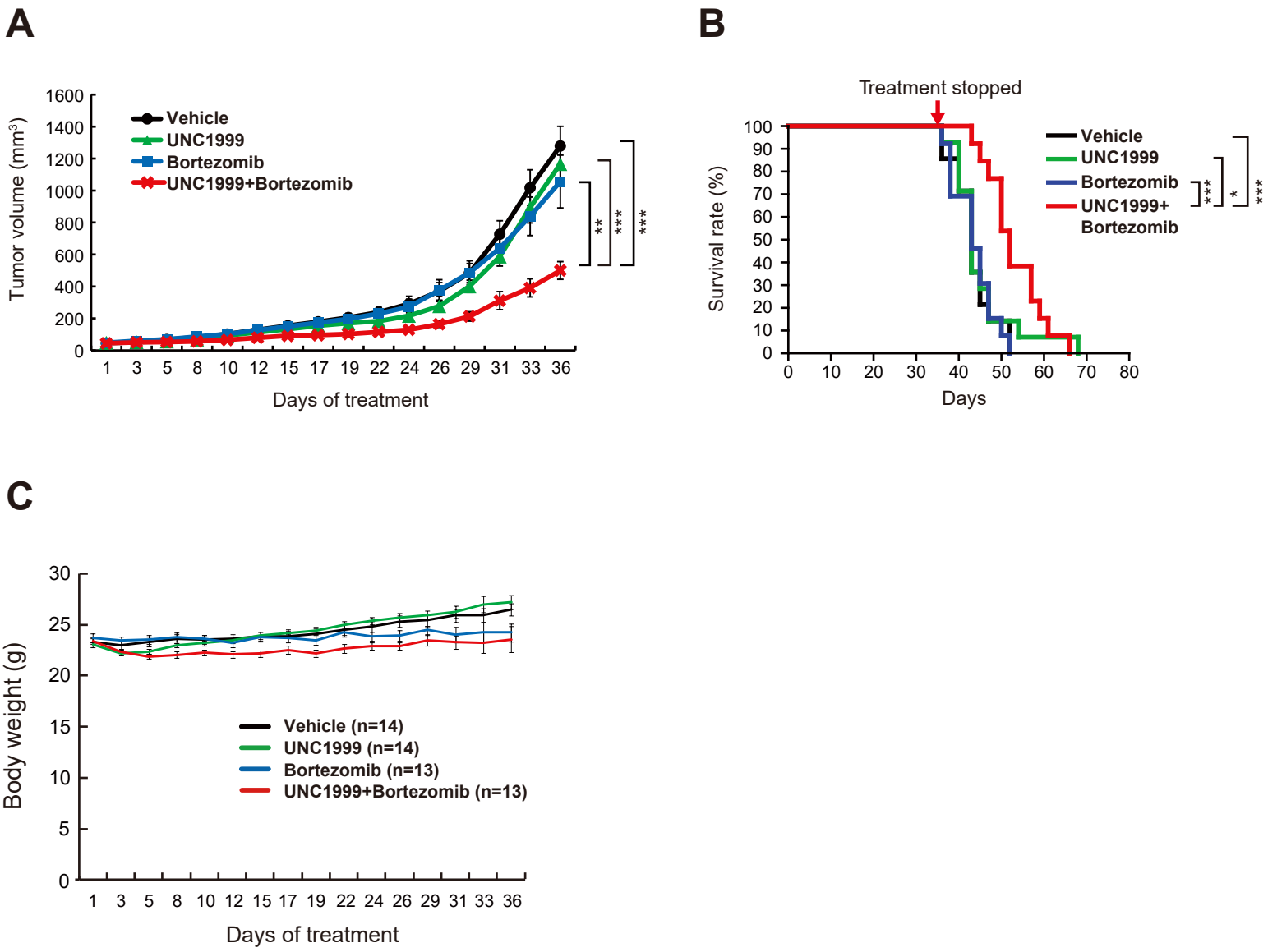
A
Tumor volume (mm³)
Vehicle
UNC1999
Bortezomib
UNC1999+Bortezomib
**
***
***
Days of treatment
B
Treatment stopped
Survival rate (%)
Vehicle
UNC1999
Bortezomib
UNC1999+
Bortezomib
***
*
***
Days
C
Body weight (g)
Vehicle (n=14)
UNC1999 (n=14)
Bortezomib (n=13)
UNC1999+Bortezomib (n=13)
Days of treatment

# Figure 10

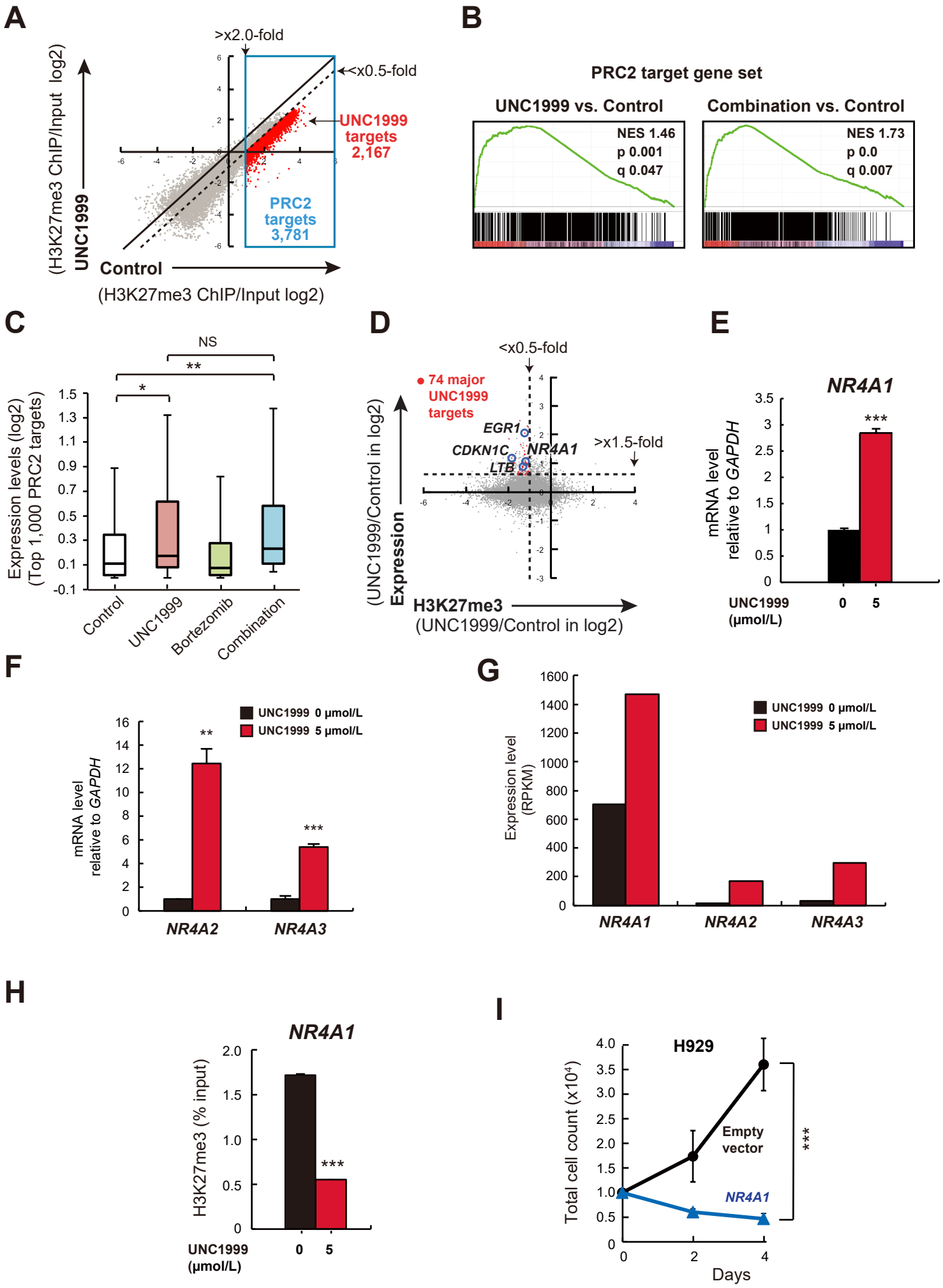
A
>x2.0-fold
<x0.5-fold
UNC1999 targets 2,167
PRC2 targets 3,781
UNC1999 (H3K27me3 ChIP/Input log2)
Control (H3K27me3 ChIP/Input log2)
B
PRC2 target gene set
UNC1999 vs. Control
NES 1.46
p 0.001
q 0.047
Combination vs. Control
NES 1.73
p 0.0
q 0.007
C
NS
**
*
Expression levels (log2) (Top 1,000 PRC2 targets)
Control
UNC1999
Bortezomib
Combination
D
<x0.5-fold
74 major UNC1999 targets
EGR1
CDKN1C
NR4A1
LTB
>x1.5-fold
(UNC1999/Control in log2) Expression
H3K27me3 (UNC1999/Control in log2)
E
NR4A1
mRNA level relative to GAPDH
***
UNC1999 (μmol/L) 0 5
F
UNC1999 0 μmol/L
UNC1999 5 μmol/L
mRNA level relative to GAPDH
**
***
NR4A2
NR4A3
G
UNC1999 0 μmol/L
UNC1999 5 μmol/L
Expression level (RPKM)
NR4A1
NR4A2
NR4A3
H
NR4A1
H3K27me3 (% input)
***
UNC1999 (μmol/L) 0 5
I
H929
Total cell count (x10⁴)
Empty vector
NR4A1
***
Days

# Figure 11

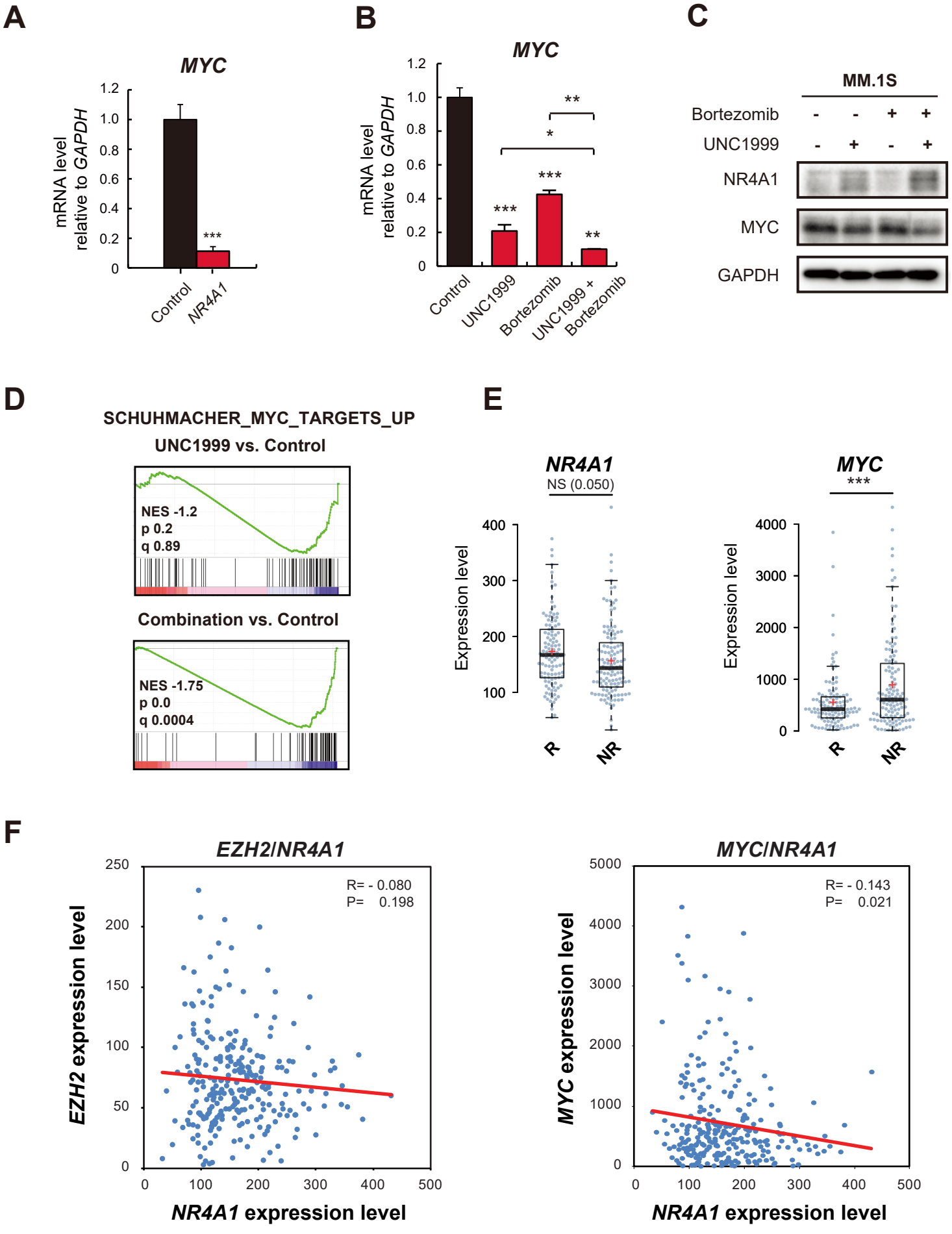
A
MYC
mRNA level relative to GAPDH
1.2
1.0
0.8
0.6
0.4
0.2
0
***
Control
NR4A1
B
MYC
mRNA level relative to GAPDH
1.2
1.0
0.8
0.6
0.4
0.2
0
**
*
***
***
**
Control
UNC1999
Bortezomib
UNC1999 + Bortezomib
C
MM.1S
Bortezomib - - + +
UNC1999 - + - +
NR4A1
MYC
GAPDH
D
SCHUHMACHER_MYC_TARGETS_UP
UNC1999 vs. Control
NES -1.2
p 0.2
q 0.89
Combination vs. Control
NES -1.75
p 0.0
q 0.0004
E
NR4A1
NS (0.050)
Expression level
400
300
200
100
R
NR
MYC
***
Expression level
4000
3000
2000
1000
0
R
NR
F
EZH2/NR4A1
EZH2 expression level
250
200
150
100
50
0
R= - 0.080
P= 0.198
0
100
200
300
400
500
NR4A1 expression level
MYC/NR4A1
MYC expression level
5000
4000
3000
2000
1000
0
R= - 0.143
P= 0.021
0
100
200
300
400
500
NR4A1 expression level

# Figure 12

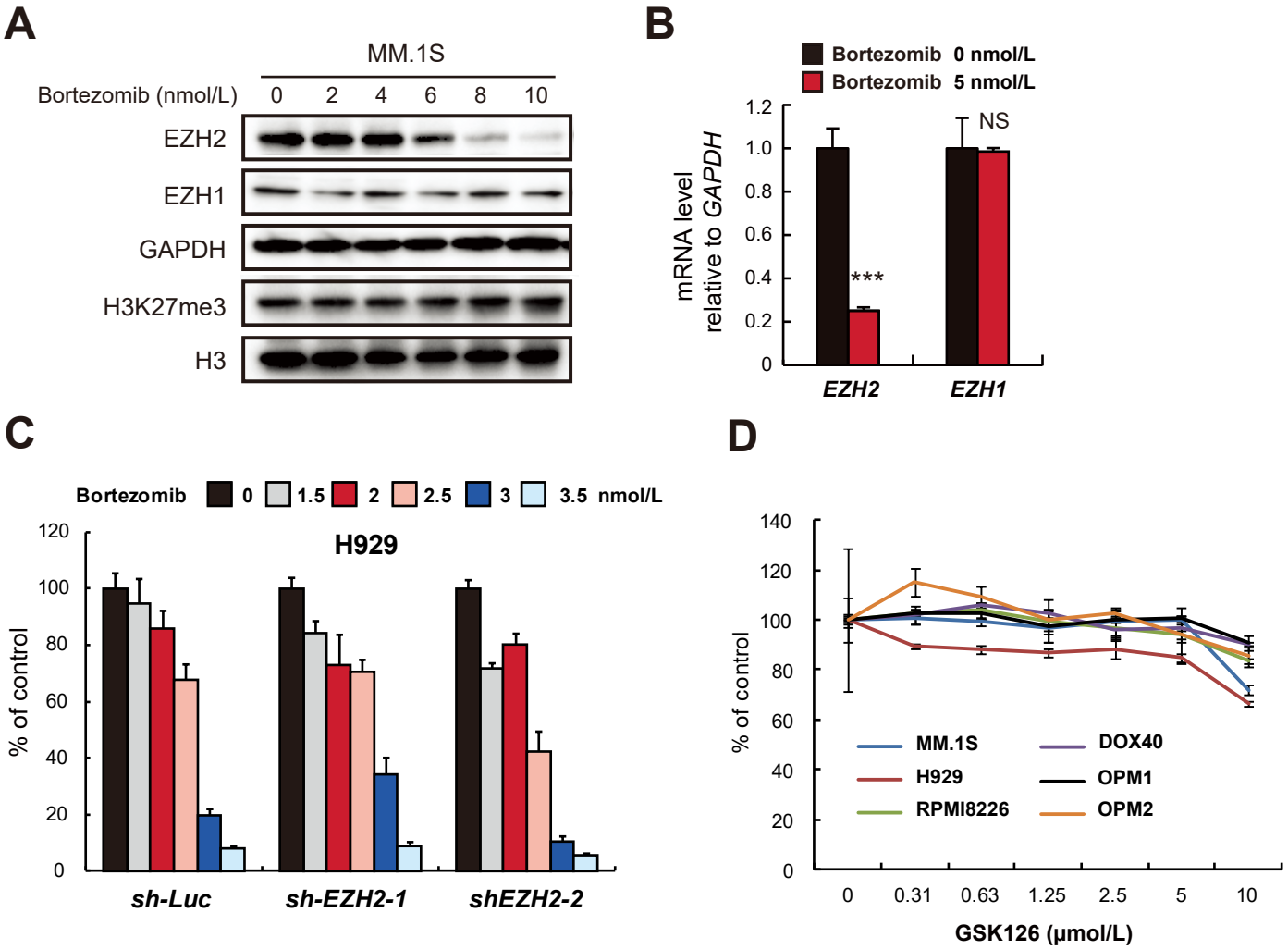
A
MM.1S
Bortezomib (nmol/L) 0 2 4 6 8 10
EZH2
EZH1
GAPDH
H3K27me3
H3
B
Bortezomib 0 nmol/L
Bortezomib 5 nmol/L
mRNA level relative to GAPDH
1.2
1.0
0.8
0.6
0.4
0.2
0
NS
***
EZH2
EZH1
C
Bortezomib 0 1.5 2 2.5 3 3.5 nmol/L
H929
% of control
120
100
80
60
40
20
0
sh-Luc
sh-EZH2-1
shEZH2-2
D
% of control
140
120
100
80
60
40
20
0
MM.1S
H929
RPMI8226
DOX40
OPM1
OPM2
0 0.31 0.63 1.25 2.5 5 10
GSK126 (μmol/L)

# Figure 13

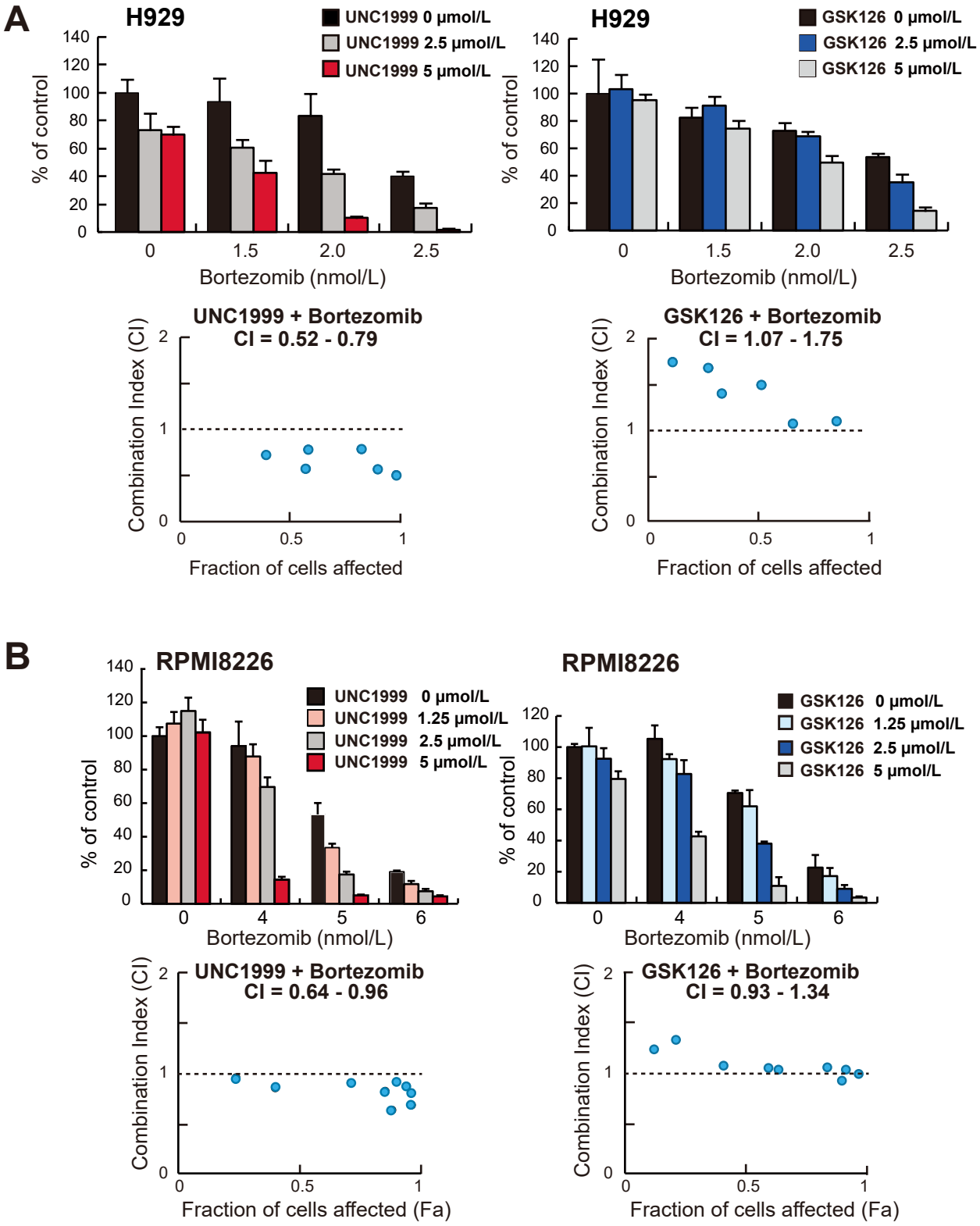
A
H929
UNC1999 0 μmol/L
UNC1999 2.5 μmol/L
UNC1999 5 μmol/L
% of control
Bortezomib (nmol/L)
H929
GSK126 0 μmol/L
GSK126 2.5 μmol/L
GSK126 5 μmol/L
UNC1999 + Bortezomib
CI = 0.52 - 0.79
Combination Index (CI)
Fraction of cells affected
GSK126 + Bortezomib
CI = 1.07 - 1.75
B
RPMI8226
UNC1999 0 μmol/L
UNC1999 1.25 μmol/L
UNC1999 2.5 μmol/L
UNC1999 5 μmol/L
RPMI8226
GSK126 0 μmol/L
GSK126 1.25 μmol/L
GSK126 2.5 μmol/L
GSK126 5 μmol/L
UNC1999 + Bortezomib
CI = 0.64 - 0.96
Fraction of cells affected (Fa)
GSK126 + Bortezomib
CI = 0.93 - 1.34

C

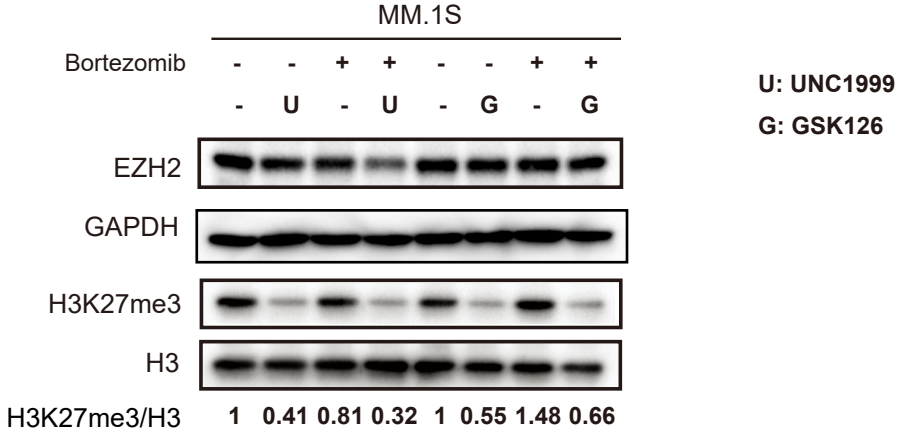
MM.1S
Bortezomib
U: UNC1999
G: GSK126
EZH2
GAPDH
H3K27me3
H3
H3K27me3/H3
1 0.41 0.81 0.32 1 0.55 1.48 0.66

# Figure 14

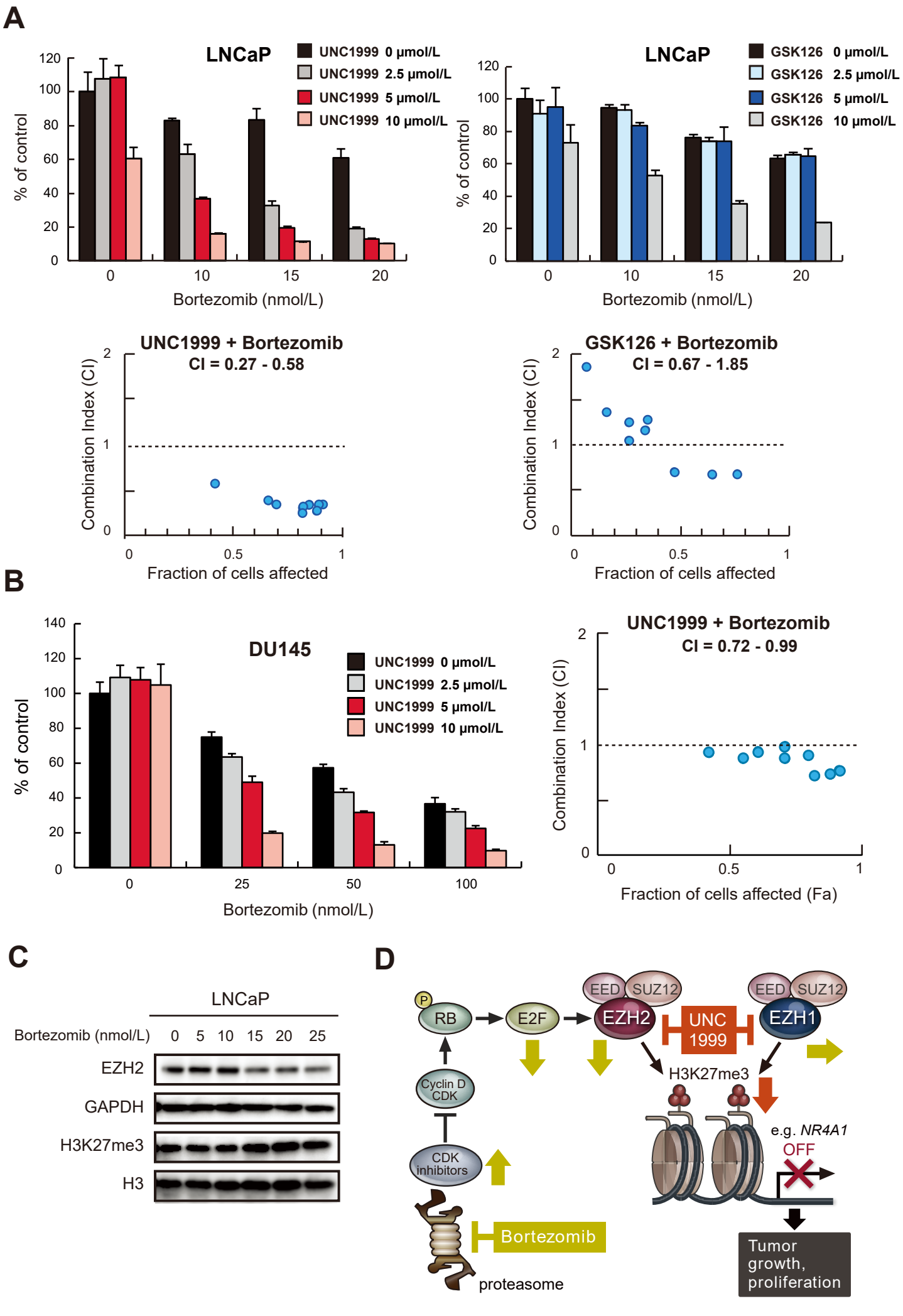
A
LNCaP
UNC1999 0 μmol/L
UNC1999 2.5 μmol/L
UNC1999 5 μmol/L
UNC1999 10 μmol/L
% of control
Bortezomib (nmol/L)
LNCaP
GSK126 0 μmol/L
GSK126 2.5 μmol/L
GSK126 5 μmol/L
GSK126 10 μmol/L
% of control
Bortezomib (nmol/L)
UNC1999 + Bortezomib
CI = 0.27 - 0.58
Combination Index (CI)
Fraction of cells affected
GSK126 + Bortezomib
CI = 0.67 - 1.85
Combination Index (CI)
Fraction of cells affected
B
DU145
UNC1999 0 μmol/L
UNC1999 2.5 μmol/L
UNC1999 5 μmol/L
UNC1999 10 μmol/L
% of control
Bortezomib (nmol/L)
UNC1999 + Bortezomib
CI = 0.72 - 0.99
Combination Index (CI)
Fraction of cells affected (Fa)
C
LNCaP
Bortezomib (nmol/L) 0 5 10 15 20 25
EZH2
GAPDH
H3K27me3
H3
D
RB
E2F
EED
SUZ12
EZH2
UNC 1999
EED
SUZ12
EZH1
H3K27me3
Cyclin D CDK
CDK inhibitors
Bortezomib
proteasome
e.g. NR4A1
OFF
Tumor growth, proliferation

**Table 1. Combination index (CI) values.**

The combined effect of two agents was analyzed by isobologram analysis using the Compu-Syn software program (ComboSyn, Inc).

**(A)** Combination index (CI) values in H929 cells treated with the combination of UNC1999 and bortezomib.

**(B)** Combination index (CI) values in MM.1S cells treated with the combination of UNC1999 and carfilzomib.

**(C)** Combination index (CI) values in RPMI8226 cells treated with the combination of UNC1999 and bortezomib.

**(D)** Combination index (CI) values in DOX40 cells treated with the combination of UNC1999 and bortezomib.

**(E)** Combination index (CI) values in MM.1S cells treated with the combination of UNC1999 and bortezomib in the presence of normal media or conditioned media derived from bone marrow stromal cells (BMSCs).

**(F)** Combination index (CI) values in H929 cells treated with bortezomib in combination with UNC1999 or GSK126.

**(G)** Combination index (CI) values in RPMI8226 cells treated with bortezomib in combination with UNC1999 or GSK126.

**(H)** Combination index (CI) values in LNCaP cells treated with bortezomib in combination with UNC1999 or GSK126.

**(I)** Combination index (CI) values in DU145 cells treated with bortezomib in combination with UNC1999.

**Table 1A**

| Bortezomib (nmol/L) | UNC1999 (μmol/L) | Fraction of cells affected (Fa) | CI |
|---|---|---|---|
| 1.5 | 2.5 | 0.3487 | 0.8905 |
| 1.5 | 5.0 | 0.4938 | 0.4291 |
| 2.0 | 2.5 | 0.3585 | 0.9820 |
| 2.0 | 5.0 | 0.6245 | 0.4247 |
| 2.5 | 2.5 | 0.4815 | 0.7245 |
| 2.5 | 5.0 | 0.9176 | 0.1978 |

**Table 1B**

| Carfilzomib (nmol/L) | UNC1999 (μmol/L) | Fraction of cells affected (Fa) | CI |
|---|---|---|---|
| 3.0 | 1.25 | 0.4866 | 0.9434 |
| 3.0 | 2.5 | 0.8314 | 0.5910 |
| 3.0 | 5.0 | 0.9269 | 0.4738 |
| 4.0 | 1.25 | 0.7334 | 0.8531 |
| 4.0 | 2.5 | 0.8296 | 0.7625 |
| 4.0 | 5.0 | 0.9150 | 0.6399 |
| 5.0 | 1.25 | 0.8806 | 0.7891 |
| 5.0 | 2.5 | 0.8842 | 0.8113 |
| 5.0 | 5.0 | 0.9512 | 0.6444 |

**Table 1C**

| Bortezomib (nmol/L) | UNC1999 (μmol/L) | Fraction of cells affected (Fa) | CI |
|---|---|---|---|
| 4.0 | 2.5 | 0.2878 | 0.9819 |
| 4.0 | 5.0 | 0.5691 | 0.7992 |
| 5.0 | 2.5 | 0.5631 | 0.9220 |
| 5.0 | 5.0 | 0.8108 | 0.7432 |
| 6.0 | 2.5 | 0.7791 | 0.8921 |
| 6.0 | 5.0 | 0.8938 | 0.7673 |

**Table 1D**

| Bortezomib (nmol/L) | UNC1999 (μmol/L) | Fraction of cells affected (Fa) | CI |
|---|---|---|---|
| 10.0 | 1.25 | 0.4036 | 0.9349 |
| 12.5 | 1.25 | 0.6916 | 0.8849 |
| 15.0 | 1.25 | 0.8100 | 0.9226 |
| 10.0 | 2.5 | 0.6414 | 0.7518 |
| 12.5 | 2.5 | 0.8332 | 0.7446 |
| 15.0 | 2.5 | 0.8982 | 0.7894 |
| 10.0 | 5.0 | 0.8422 | 0.5904 |
| 12.5 | 5.0 | 0.8390 | 0.7406 |
| 15.0 | 5.0 | 0.8595 | 0.8567 |

**Table 1E**

| Bortezomib (nmol/L) | UNC1999 (μmol/L) | Normal medium | | BMSC medium | |
|---|---|---|---|---|---|
| | | Fraction of cells affected (Fa) | CI | Fraction of cells affected (Fa) | CI |
| 1.5 | 2.5 | 0.5132 | 1.2122 | 0.4711 | 1.0066 |
| 1.5 | 5 | 0.8326 | 0.8513 | 0.5918 | 0.8837 |
| 2 | 2.5 | 0.8336 | 0.9733 | 0.5250 | 1.0838 |
| 2 | 5 | 0.9288 | 0.8949 | 0.8160 | 0.7230 |
| 2.5 | 2.5 | 0.9043 | 1.1016 | 0.7168 | 0.9897 |
| 2.5 | 5 | 0.9505 | 1.0516 | 0.8860 | 0.8032 |

**Table 1F**

| Bortezomib (nmol/L) | UNC1999 or GSK126 (μmol/L) | UNC1999 | | GSK126 | |
|---|---|---|---|---|---|
| | | Fraction of cells affected (Fa) | CI | Fraction of cells affected (Fa) | CI |
| 1.5 | 2.5 | 0.3933 | 0.7361 | 0.1168 | 1.7449 |
| 1.5 | 5.0 | 0.5720 | 0.5909 | 0.2767 | 1.6843 |
| 2.0 | 2.5 | 0.5815 | 0.7783 | 0.3345 | 1.4023 |
| 2.0 | 5.0 | 0.8981 | 0.5689 | 0.5177 | 1.4984 |
| 2.5 | 2.5 | 0.8233 | 0.7916 | 0.6617 | 1.0746 |
| 2.5 | 5.0 | 0.9823 | 0.5217 | 0.8597 | 1.0958 |

**Table 1G**

| Bortezomib (nmol/L) | UNC1999 or GSK126 (μmol/L) | UNC1999 | | GSK126 | |
|---|---|---|---|---|---|
| | | Fraction of cells affected (Fa) | CI | Fraction of cells affected (Fa) | CI |
| 4.0 | 1.25 | 0.2359 | 0.9560 | 0.1237 | 1.2524 |
| 4.0 | 2.5 | 0.3942 | 0.8674 | 0.2145 | 1.3443 |
| 4.0 | 5.0 | 0.8752 | 0.6364 | 0.5949 | 1.0580 |
| 5.0 | 1.25 | 0.7090 | 0.9129 | 0.4114 | 1.0679 |
| 5.0 | 2.5 | 0.8481 | 0.8194 | 0.6393 | 1.0383 |
| 5.0 | 5.0 | 0.9562 | 0.6861 | 0.8971 | 0.9307 |
| 6.0 | 1.25 | 0.8976 | 0.9272 | 0.8372 | 1.0595 |
| 6.0 | 2.5 | 0.9351 | 0.8691 | 0.9145 | 1.0373 |
| 6.0 | 5.0 | 0.9619 | 0.8079 | 0.9678 | 0.9967 |

**Table 1H**

| Bortezomib (nmol/L) | UNC1999 or GSK126 (μmol/L) | UNC1999 | | GSK126 | |
|---|---|---|---|---|---|
| | | Fraction of cells affected (Fa) | CI | Fraction of cells affected (Fa) | CI |
| 10.0 | 2.5 | 0.4179 | 0.5805 | 0.0696 | 1.8518 |
| 10.0 | 5.0 | 0.6637 | 0.3916 | 0.1637 | 1.3510 |
| 10.0 | 10.0 | 0.8513 | 0.3629 | 0.4715 | 0.7031 |
| 15.0 | 2.5 | 0.6991 | 0.3536 | 0.2634 | 1.0669 |
| 15.0 | 5.0 | 0.8198 | 0.3018 | 0.2615 | 1.2375 |
| 15.0 | 10.0 | 0.8943 | 0.3398 | 0.6492 | 0.6647 |
| 20.0 | 2.5 | 0.8234 | 0.2735 | 0.3447 | 1.1812 |
| 20.0 | 5.0 | 0.8788 | 0.2693 | 0.3525 | 1.2707 |
| 20.0 | 10.0 | 0.9058 | 0.3491 | 0.7609 | 0.6902 |

**Table 1I**

| Bortezomib (nmol/L) | UNC1999 (μmol/L) | Fraction of cells affected (Fa) | CI |
|---|---|---|---|
| 25 | 1.25 | 0.4186 | 0.9347 |
| 25 | 2.5 | 0.5510 | 0.8718 |
| 25 | 5.0 | 0.8185 | 0.7163 |
| 50 | 1.25 | 0.6036 | 0.9484 |
| 50 | 2.5 | 0.7099 | 0.8802 |
| 50 | 5.0 | 0.8801 | 0.7360 |
| 100 | 1.25 | 0.7067 | 0.9934 |
| 100 | 2.5 | 0.7937 | 0.9061 |
| 100 | 5.0 | 0.9106 | 0.7647 |

**Table 2. Significantly upregulated PRC2 gene sets in UNC1999-treated MM.1S cells.**

Gene set enrichment analysis (GSEA) using our RNA-seq data identified PRC2 target gene sets that are significantly enriched in UNC1999-treated MM.1S cells (FDR q-value <0.05).

| NAME | SIZE | NES | NOM p-val | FDR q-val |
|---|---|---|---|---|
| AGM_VE-CAD+CD45+ VS ABM_150+34-LSK UPON TOP500 2012 | 408 | 1.8839391 | 0 | 0.004089887 |
| EZH2KO_SASHIDA_ABM_BMT_E2KO VS WT_UPON | 543 | 1.844744 | 0 | 0.004125951 |
| PLACENTA_45+KIT+CD34MED VS ABM_150+34-LSK UPON TOP500 2012 | 428 | 1.8432679 | 0 | 0.003615148 |
| EZH1_2_OLA_UNC1999_MM.1S_K27ME3_GR_3FOLD | 2742 | 1.7841836 | 0 | 0.008655357 |
| UNC1999_CHIP_K27_TARGET_IN_PRC2_TARGET_OLA_MM.1S | 2050 | 1.7660209 | 0 | 0.011018296 |
| H2AK119UB1_WT-GMP > 5FOLD 766GENES | 699 | 1.7608407 | 0 | 0.010083644 |
| EZH1_2_OLA_UNC1999_MM.1S_K27ME3_GR_4FOLD | 2156 | 1.7555077 | 0 | 0.009016174 |
| EZH1_2_OLA_UNC1999_MM.1S_K27ME3_GR_2FOLD | 3601 | 1.7482537 | 0 | 0.00856214 |
| EZH2KOTET2KD_MUTO_FL-BMT_LSK_DKO VS WT UPON | 237 | 1.7156032 | 0 | 0.013547997 |
| EZH2KO_MUTO_FL-BMT_LSK_E2KO VS WT UPON | 367 | 1.711354 | 0 | 0.012982707 |
| H2AK119UB1_WT-GMP > 4FOLD 1859GENES | 1684 | 1.696451 | 0 | 0.015298391 |
| EZH2KOTET2KD-MDS_MUTO_FL-BMT_GMP_ET77 VS WT UPON | 796 | 1.6943446 | 0 | 0.014246338 |
| EZH2KO_SASHIDA_AHSCVECTOR_BMT_1000_E2KO VS WT_UPON | 674 | 1.6850624 | 0 | 0.014819628 |
| CD34-LSK_SPECIFIC GEROGE-ARRAY UPON | 546 | 1.6674124 | 0 | 0.018670889 |
| TET2KD_MUTO_FL-BMT_GMP_T2KD VS WT UPON | 116 | 1.660364 | 0.003194888 | 0.019254837 |
| MPP_SPECIFIC GEROGE-RNA-SEQ | 108 | 1.6446334 | 0.001675042 | 0.022012768 |
| MONOCYTES_GOODEL | 64 | 1.6385078 | 0.013445378 | 0.022561245 |
| PRC2-TARGET IN ABM-GMP K27ME3 > 4FOLD_3859GENES | 1979 | 1.6372403 | 0 | 0.021678675 |
| LSKCD34- VS MPPFLK2+,- UPON 2014_ROSSI | 204 | 1.618182 | 0.001718213 | 0.025311075 |
| EZH2KO-MDS_CASCIO_DNOFF_B10-F14 | 948 | 1.6119399 | 0.001321004 | 0.02553239 |
| TET2KD_MUTO_FL-BMT_LSK_T2KD VS WT UPON | 284 | 1.6050408 | 0.001644737 | 0.02650931 |
| PRC2-TARGET IN ABM-LK K27ME3 > 2FOLD_3773GENES | 1983 | 1.600118 | 0 | 0.027115148 |
| EZH2KOTET2KD-MDS_MUTO_FL-BMT_GMP_ET70 VS WT UPON | 761 | 1.5943123 | 0 | 0.02759404 |
| SOX17 OE CD48LSK-DEV-WT UP 376GENES 2011_MORRISON | 292 | 1.593092 | 0 | 0.026844835 |
| EZH1_2_OLA_UNC1999_MM.1S_K27ME3_GR_TOP1000 | 960 | 1.5877097 | 0 | 0.027534094 |
| H2AK119UB1_WT-LSK > 2FOLD 3946GENES | 1916 | 1.5817297 | 0 | 0.028337164 |
| NK CELLS_GOODEL | 45 | 1.5793766 | 0.021812081 | 0.027997788 |
| PRC2-TARGET IN ABM-BMT-LSK K27ME3_TOP500GENES | 472 | 1.5725046 | 0 | 0.0288503 |
| PRC2-TARGET IN BMT-LSK_HASEGAWA_K27 > 2FOLD_LSK-WT_4107GENES | 1854 | 1.5693363 | 0 | 0.02906221 |
| 2008-ORKIN_ESC_EZH1_K27-EZH2KO_EZH1-EZH2KO | 189 | 1.5691547 | 0.003284072 | 0.028240241 |
| EZH2KO_MUTO_FL-BMT_GMP_EZH2KO VS WT UPON | 356 | 1.5592595 | 0 | 0.03015549 |
| PRC2-TARGET IN ABM-BMT-LSK K27ME3 > 2FOLD_2917GENES | 1933 | 1.5576934 | 0 | 0.029507585 |
| EEDKO VS WT BM_LT-HSC UP > 3FOLD 339GENES S2N 2014_ORKIN | 302 | 1.5497996 | 0.001584786 | 0.031300623 |
| EZH2KO-MDS_CASCIO_DNOFF_B11-F2 | 1019 | 1.5446994 | 0 | 0.031929474 |
| BIVALENT IN FL-BMT-LSK_HASEGAWA_LSK-WT_K27ME3 > 2FOLD_K4ME3 > 1.5FOLD_1883GENES | 1671 | 1.5433587 | 0 | 0.031772 |
| EZH2KO-1M_K27_WT > 2_EZH2KO-VS-WT > 0.8_AOYAMA | 526 | 1.5422975 | 0 | 0.03124281 |
| EZH2KO-MDS-PLTHIGH_CASCIO_DNOFF_B10-F7 | 1539 | 1.542072 | 0 | 0.030435225 |
| EZH2KO_MUTO_FL-BMT_GMP_E2KO VS WT UPON | 345 | 1.5357662 | 0 | 0.031231508 |
| EZH2KOTET2KD-MDS_MUTO_FL-BMT_LSK_E19 VS WT DNOFF | 640 | 1.5337346 | 0 | 0.030878479 |
| EZH2KO-MDSMPN_CASCIO_DNOFF_B11-F5 | 1434 | 1.5283102 | 0 | 0.03211698 |
| EZH2KO-MDSMPN-2NDBMT_CASCIO_DNOFF_B10F52-F2 | 2580 | 1.5259757 | 0 | 0.032148264 |
| H2AK119UB1_WT-LSK > 3.5FOLD 729GENES | 686 | 1.5228395 | 0 | 0.032327462 |
| EZH2KO-1M_K27_WT > 2_EZH2KO-VS-WT < 0.5_AOYAMA | 1529 | 1.5196855 | 0 | 0.032762982 |
| EZH2TARGET IN FL-BMT-LSK_HASEGAWA_LSK_CHIP_K27_WT > 2_EZH2KO VS WT < 1__MUTO-LSK_EXP_EZH2KO VS WT-UP,ON_31GENES | 772 | 1.5169932 | 0 | 0.032860067 |
| 2008-ORKIN_ESC_EZH2_K27-WT_NOK27-EZH2KO | 589 | 1.5149614 | 0.002890173 | 0.0330029 |
| SOX17 OE HSCS-DEV-WT UP TOP500 2011_MORRISON | 414 | 1.5130467 | 0.00309119 | 0.033010162 |
| BIVALENT_SP_LSKCD150-_K27ME3 > 3FOLD_K4ME3 > 10FOLD_04MO_CHIP-SEQ_2014_GOODELL_GSE47819_1157GENES | 2229 | 1.5080268 | 0 | 0.03377041 |
| BMI1-KO_LSK DOWN OGURO | 238 | 1.5073092 | 0.007849294 | 0.03332933 |
| PRC2_EZH2KO-1M_K27_WT > 3_AOYAMA | 2521 | 1.5071855 | 0 | 0.032679573 |

| | | | | |
|---|---|---|---|---|
| PRC2-TARGET IN ABM-LSK K27ME3_TOP1000GENES | 2210 | 1.5023953 | 0 | 0.033841066 |
| TET2KD_MUTO_FL-BMT_GMP_T2KD VS WT DNOFF | 229 | 1.4862456 | 0.01821192 | 0.039234105 |
| EZH2KOTET2KD_MUTO_FL-BMT_GMP_DKO VS WT UPON | 356 | 1.482786 | 0.007496252 | 0.039773364 |
| PRC2-TARGET IN ABM-LSK K27ME3 > 2FOLD_3192GENES | 1933 | 1.4823841 | 0 | 0.039180823 |
| BIVALENT IN FL-BMT-LSK_HASEGAWA_LSK-WT_K27ME3 > 2FOLD_K4ME3 > 2FOLD_759GENES | 666 | 1.4818178 | 0.001410437 | 0.03864862 |
| LTHSC_SPECIFIC GEROGE-RNA-SEQ | 258 | 1.4690437 | 0.012820513 | 0.04274336 |
| PRC2-TARGET IN ABM-GMP K27ME3_TOP500GENES | 1021 | 1.4656227 | 0 | 0.043372106 |
| FL_13-5_150+48-LSK VS ABM_150+34-LSK DOWNOFF TOP500 2012 | 387 | 1.459586 | 0.006097561 | 0.045752805 |
| SOX17 OE HSCS-DEV-WT UP TOP100 2011_MORRISON | 86 | 1.4572768 | 0.0352349 | 0.045787722 |
| EZH2KO-MDSMPNQ_CASCIO_DNOFF_F2 | 1584 | 1.4562854 | 0.001298701 | 0.04541264 |
| EZH1_2_OLA_UNC1999_MM.1S_K27ME3_GR_TOP500 | 483 | 1.4529027 | 0.012102874 | 0.046120077 |
| EZH2KO_MUTO_FL-BMT_GMP_E2KO VS WT DNOFF | 154 | 1.4492344 | 0.026533997 | 0.046714045 |
| MUTO_GMP-K27_KO VS WT-0.5_WT-3 UP ON | 118 | 1.4412801 | 0.03642384 | 0.04965807 |
| HSC_GOODEL | 207 | 1.4410642 | 0.014128729 | 0.048914943 |

**Table 3. Significantly upregulated PRC2 gene sets in combination-treated MM.1S cells.**

Gene set enrichment analysis (GSEA) using our RNA-seq data identified PRC2 target gene sets that are significantly enriched in MM.1S cells treated with the combination of UNC1999 and bortezomib (FDR q-value <0.05).

| NAME | SIZE | NES | NOM p-val | FDR q-val |
|---|---|---|---|---|
| EZH1_2_OLA_UNC1999_MM.1S_K27ME3_GR_TOP1000 | 960 | 2.038131 | 0 | 0 |
| TET2KD_MUTO_FL-BMT_GMP_T2KD VS WT UPON | 116 | 1.993437 | 0 | 0 |
| BMI1-KO_LSK DOWN OGURO | 238 | 1.915446 | 0 | 0 |
| AGM_VE-CAD+CD45+ VS ABM_150+34-LSK UPON TOP500 2012 | 408 | 1.756663 | 0 | 0.004732331 |
| TET2KD_MUTO_FL-BMT_LSK_T2KD VS WT UPON | 284 | 1.785852 | 0 | 0.005046993 |
| EZH2KO_SASHIDA_ABM_BMT_E2KO VS WT_UPON | 543 | 1.733326 | 0 | 0.005595749 |
| EZH2KO-MDS_CASCIO_DNOFF_B10-F14 | 948 | 1.703561 | 0 | 0.006477696 |
| EZH1_2_OLA_UNC1999_MM.1S_K27ME3_GR_TOP500 | 483 | 1.739494 | 0 | 0.006528374 |
| PLACENTA_45+KIT+CD34MED VS ABM_150+34-LSK UPON TOP500 2012 | 428 | 1.716587 | 0 | 0.006957409 |
| EZH2KOTET2KD-MDS_MUTO_FL-BMT_LSK_E19 VS WT DNOFF | 640 | 1.611375 | 0 | 0.024427976 |
| EZH2KO-MDS_CASCIO_DNOFF_B11-F2 | 1019 | 1.557241 | 0 | 0.02966724 |
| EZH2KOTET2KD-MDS_MUTO_FL-BMT_GMP_ET77 VS WT UPON | 796 | 1.562724 | 0 | 0.030288149 |
| EZH2KOTET2KD_MUTO_FL-BMT_LSK_DKO VS WT UPON | 237 | 1.576857 | 0 | 0.031208133 |
| EZH1_2_OLA_UNC1999_MM.1S_K27ME3_GR_10FOLD | 252 | 1.541668 | 0 | 0.03150973 |
| EZH2KO_SASHIDA_AHSCVECTOR_BMT_1000_E2KO VS WT_UPON | 674 | 1.531724 | 0 | 0.032200407 |
| EEDKO VS WT BM_LT-HSC UP > 3FOLD 339GENES S2N 2014_ORKIN | 302 | 1.565611 | 0 | 0.03236416 |
| EZH2KO_MUTO_FL-BMT_LSK_E2KO VS WT UPON | 367 | 1.577626 | 0 | 0.03377251 |
| MPP_SPECIFIC GEROGE-RNA-SEQ | 108 | 1.509353 | 0 | 0.03621907 |
| EZH2KO-MDSMPN_CASCIO_DNOFF_B11-F5 | 1434 | 1.373092 | 0 | 0.09662716 |
| BRUECKNER_TARGETS_OF_MIRLET7A3_UP | 105 | 1.366569 | 0.021978023 | 0.09736389 |
| LSKCD34- VS MPPFLK2+,- UPON 2014_ROSSI | 204 | 1.336189 | 0.013888889 | 0.10865448 |
| MONOCYTES_GOODEL | 64 | 1.337015 | 0.052173913 | 0.11252609 |
| EZH2KO-MDS-PLTHIGH_CASCIO_DNOFF_B10-F7 | 1539 | 1.341122 | 0 | 0.11508455 |
| CD34-LSK_SPECIFIC GEROGE-ARRAY UPON | 546 | 1.282573 | 0 | 0.14296083 |
| MUTO_GMP-K27_KO VS WT-0.5_WT-3 UP ON | 118 | 1.282721 | 0.03508772 | 0.14867927 |
| BRUECKNER_TARGETS_OF_MIRLET7A3_DN | 77 | 1.288889 | 0.08050848 | 0.14956464 |
| EZH2KOTET2KD-MDS_MUTO_FL-BMT_GMP_ET70 VS WT UPON | 761 | 1.232986 | 0 | 0.19677146 |
| H2AK119UB1_WT-LSK > 3.5FOLD 729GENES | 686 | 1.223329 | 0 | 0.20442982 |
| LTHSC_SPECIFIC GEROGE-RNA-SEQ | 258 | 1.216009 | 0.046511628 | 0.20876718 |
| BCORKO VS WT UPON BMT_LSK TANAKA_RNA-SEQ > 2FOLD_1INFLATE | 769 | 1.201469 | 0 | 0.21420543 |
| EZH2KO_MUTO_FL-BMT_GMP_E2KO VS WT DNOFF | 154 | 1.204074 | 0.10191083 | 0.21776149 |
| EZH2KOTET2KD-MDS_MUTO_FL-BMT_LSK_E18 VS WT DNOFF | 703 | 1.187042 | 0 | 0.23063451 |
| H2AK119UB1_WT-GMP > 5FOLD 766GENES | 699 | 1.182274 | 0 | 0.23166198 |
| EZH2KO-MDSMPNQ_CASCIO_DNOFF_F2 | 1584 | 1.162218 | 0 | 0.26081526 |
| 21MO VS 12MO UPON SPARKLS ARRAY 2007_GOODELL | 128 | 1.135571 | 0.16477273 | 0.2724012 |
| CEBPA-KD_HSCS UP TOP100 TENEN 2013_D7 | 67 | 1.150959 | 0.19026549 | 0.27343008 |
| HUMANHSCS OLD VS YOUNG UP S2N TOP100 GSE32719 | 93 | 1.131766 | 0.2292683 | 0.2738723 |
| FL_14-5_150+48-LSK VS ABM_150+34-LSK DOWNOFF TOP500 2012 | 398 | 1.139702 | 0.06 | 0.27811852 |
| 24MO VS 04MO UP TOP100 S2N SPLSKCD150- RNA-SEQ 2014_GOODELL | 91 | 1.143477 | 0.17821783 | 0.2786928 |
| EZH2KO_MUTO_FL-BMT_GMP_E2KO VS WT UPON | 345 | 1.135812 | 0.060606062 | 0.2788061 |
| SOX17 OE CD48LSK-DEV-WT UP 376GENES 2011_MORRISON | 292 | 1.119467 | 0.11494253 | 0.28373903 |
| FL_13-5_150+48-LSK VS ABM_150+34-LSK DOWNOFF TOP500 2012 | 387 | 1.113986 | 0.06153846 | 0.28644598 |
| PRC2-TARGET IN ABM-BMT-LSK K27ME3_TOP500GENES | 472 | 1.120644 | 0.04 | 0.28878835 |
| EZH2KO_MUTO_FL-BMT_GMP_EZH2KO VS WT UPON | 356 | 1.107892 | 0.12820514 | 0.29353318 |
| EZH2KO-1M_K27_WT > 2_EZH2KO-VS-WT > 0.8_AOYAMA | 526 | 1.103432 | 0.121212125 | 0.2957095 |
| FL_12-5_VE-CAD+MAC1LOWLSK VS ABM_150+34-LSK DOWNOFF TOP500 2012 | 371 | 1.054261 | 0.12698413 | 0.41266543 |
| CEBPA-KD_HSCS DOWN TOP500 TENEN 2013_D7 | 385 | 1.050906 | 0.25 | 0.41538653 |
| EEDKO VS WT BM_LT-HSC UP < 0.33FOLD 109GENES S2N 2014_ORKIN | 82 | 1.037325 | 0.3517588 | 0.45100906 |
| EEDKO VS WT BM_LT-HSC UP TOP500 S2N 2014_ORKIN | 452 | 1.033632 | 0.23076923 | 0.4516356 |

**Table 4. Top 74 PRC2 genes that are significantly altered in UNC1999-treated MM.1S cells.**

Within PRC2 target genes, we defined genes that showed more than 2-fold reduction in H3K27me3 levels in UNC1999-treated MM.1S cells compared with DMSO-treated cells as "UNC1999 target genes". Among these genes, we selected 74 genes with significantly enhanced expression (>1.5-fold UNC1999/Control) and remarkable reduction of H3K27me3 (≥2-fold) as major UNC1999 target genes in MM.1S cells.

| Symbol | IP/Input | | H3K27me3 (UNC1999/Control) | Expression (UNC1999/Control) |
|---|---|---|---|---|
| | Control | UNC1999 | | |
| B4GALNT1 | 2.77419355 | 1.08413095 | 0.390791389 | 1.653341911 |
| PHLDA2 | 9.4789916 | 3.74200468 | 0.394768225 | 1.79486717 |
| NOG | 2.34104046 | 1.13709042 | 0.485720106 | 1.983382414 |
| FURIN | 6.16517857 | 2.24752007 | 0.364550684 | 1.782095703 |
| PDLIM2 | 7.53278689 | 3.0464 | 0.404418716 | 2.076965762 |
| FBXO2 | 3.80882353 | 1.82589142 | 0.47938462 | 2.666123933 |
| TNFRSF12A | 4.35344828 | 1.38966513 | 0.319210208 | 2.272379776 |
| KCTD17 | 3.6875 | 1.80624361 | 0.489828775 | 1.8285526 |
| LAPTM4B | 4.06451613 | 1.59746918 | 0.393028132 | 1.524046495 |
| PTP4A3 | 5.96052632 | 2.38434138 | 0.400021953 | 2.910717623 |
| ARHGEF40 | 2.32222222 | 0.80438435 | 0.346385605 | 1.584748503 |
| TP53I11 | 6.46666667 | 2.75738223 | 0.426399314 | 1.994753911 |
| SLC2A6 | 7.45762712 | 2.22221121 | 0.297978322 | 2.023707513 |
| MAP4K4 | 2.15929204 | 0.7315565 | 0.338794607 | 1.519566467 |
| SERPINE1 | 5.5359116 | 2.57872779 | 0.465818094 | 4.916338636 |
| C4orf48 | 2.55882353 | 1.18506892 | 0.463130383 | 1.628285412 |
| ATF3 | 5.91946309 | 2.95269278 | 0.498810911 | 2.943320625 |
| IFITM2 | 8.2556391 | 3.07271442 | 0.372195826 | 3.136479332 |
| RRAD | 6.78231293 | 3.36666443 | 0.496388837 | 2.480640192 |
| CCND1 | 8.59482759 | 4.14082734 | 0.481781316 | 1.852545516 |
| FAM19A5 | 4.35294118 | 1.70203725 | 0.391008557 | 1.552949065 |
| TMEM54 | 5.29032258 | 2.33012558 | 0.440450568 | 1.99659116 |
| LTB | 9.81818182 | 3.97113341 | 0.404467292 | 1.82669 |
| BCL9L | 3.97849462 | 1.55465649 | 0.390765008 | 1.868135369 |
| NEK6 | 2.71428571 | 1.24846346 | 0.459960223 | 1.958824163 |
| BLVRB | 2.97794118 | 0.86134443 | 0.289241587 | 2.059473255 |
| EGR1 | 2.92907801 | 1.24672815 | 0.425638423 | 4.127642637 |
| TYROBP | 5.14173228 | 1.92188571 | 0.373781754 | 1.725858833 |
| NR2F2 | 3.92934783 | 1.50006169 | 0.381758438 | 1.534643348 |
| RAB31 | 3.45588235 | 1.21075153 | 0.350345123 | 1.524107525 |
| PTMS | 2.89449541 | 1.22665029 | 0.423787262 | 2.686701624 |
| SLC2A3 | 2.2556391 | 1.10033708 | 0.487816106 | 2.25861547 |
| RIMS3 | 2.27891156 | 0.80212289 | 0.351976312 | 1.509666845 |
| MX1 | 2.97356828 | 1.38537915 | 0.465897878 | 1.596811224 |
| UNC119 | 6.30882353 | 2.78851212 | 0.442001921 | 2.018590781 |
| MXRA7 | 3.68589744 | 1.56674862 | 0.425065713 | 2.480453833 |
| IFITM1 | 5.85714286 | 2.52040681 | 0.430313357 | 2.28369906 |
| PCDH1 | 4.10638298 | 1.3018166 | 0.317022696 | 2.534735604 |
| IGFBP6 | 2.25609756 | 1.01757544 | 0.451033439 | 2.016412101 |
| C9orf7 | 3.65322581 | 1.61282946 | 0.441480913 | 1.521127762 |
| WNT10B | 2.08383234 | 0.75947141 | 0.364458983 | 1.528781495 |
| TMEM158 | 5.20588235 | 1.39310252 | 0.267601614 | 1.733548817 |
| SARDH | 11.2 | 4.80102959 | 0.428663356 | 1.512089825 |
| SORL1 | 2.85555556 | 1.10830332 | 0.388121786 | 2.098696811 |
| ADAMTSL2 | 11.9512195 | 5.3077631 | 0.444118953 | 1.56281874 |
| ATP13A2 | 5.75268817 | 1.93821141 | 0.336922731 | 1.560819085 |
| IL4R | 2.09625668 | 1.01129246 | 0.482427782 | 1.534315468 |
| EGR3 | 10.3417722 | 3.63193428 | 0.351190708 | 1.503005664 |
| SMOX | 2.03797468 | 0.90615995 | 0.444637491 | 2.464241943 |

| | | | | |
|---|---|---|---|---|
| NR4A1 | 6.02083333 | 2.62618651 | 0.436183227 | 2.077228118 |
| HLA-DMB | 3.48421053 | 1.36821921 | 0.392691315 | 1.640276897 |
| MT1X | 4.75163399 | 1.73031029 | 0.364150584 | 5.592061664 |
| HOXB7 | 3.42941176 | 1.23496656 | 0.360110318 | 1.704239346 |
| RTN4RL2 | 2.67088608 | 0.68223808 | 0.255435111 | 3.593613969 |
| ZNF467 | 4.63970588 | 1.92240815 | 0.414338365 | 1.912767935 |
| PRKCB | 3.07333333 | 1.41000119 | 0.458785637 | 1.975205174 |
| LIPG | 3.79432624 | 1.82798081 | 0.481766904 | 1.665232801 |
| GSTP1 | 5.25862069 | 1.61917838 | 0.307909331 | 2.023897416 |
| SLC43A2 | 2.40186916 | 1.16254568 | 0.484017074 | 1.609368534 |
| SERINC2 | 8.60479042 | 3.76557723 | 0.437614055 | 1.646779373 |
| CDKN1C | 2.53278689 | 0.70657291 | 0.278970533 | 2.26714243 |
| SYNGR1 | 4.43103448 | 1.64330228 | 0.370861993 | 1.576066531 |
| RAB37 | 7.60769231 | 3.7459213 | 0.492386015 | 1.575599822 |
| RTN2 | 2.57608696 | 1.19716146 | 0.464720905 | 2.295885849 |
| C18orf1 | 5.29310345 | 2.41847618 | 0.456910809 | 3.045665033 |
| AHNAK | 3.23913043 | 1.56608078 | 0.483488027 | 1.881983502 |
| HLA-DPA1 | 4.85840708 | 2.20413979 | 0.453675403 | 1.799515205 |
| SERPINB6 | 3.79213483 | 1.87704561 | 0.494983879 | 2.883343692 |
| KRT17 | 6.92622951 | 3.38479742 | 0.488692645 | 3.663495099 |
| TSKU | 2.08666667 | 0.97088566 | 0.465280668 | 1.533224646 |
| LAMC1 | 2.06862745 | 0.75324202 | 0.364126472 | 1.880016543 |
| IL32 | 6.00884956 | 2.88513739 | 0.480148049 | 4.787336672 |
| CYR61 | 3.92 | 1.35632166 | 0.346000422 | 1.621716708 |
| STK32C | 6.76923077 | 2.843673 | 0.420088057 | 2.449710862 |

**Table 5. Significantly upregulated gene sets in RPMI8226 cells transduced with *EZH2* overexpressing versus empty vectors.**

Gene set enrichment analysis (GSEA) using our RNA-seq data identified gene sets that are significantly enriched in RPMI8226 cells transduced with *EZH2* overexpressing versus empty vectors. (FDR q-value <0.01).

| NAME | SIZE | NES | NOM p-val | FDR q-val |
|---|---|---|---|---|
| REACTOME_PEPTIDE_CHAIN_ELONGATION | 86 | 2.42 | 0 | 0 |
| KEGG_RIBOSOME | 87 | 2.41 | 0 | 0 |
| REACTOME_TRANSLATION | 146 | 2.41 | 0 | 0 |
| REACTOME_INFLUENZA_VIRAL_RNA_TRANSCRIPTION_AND_REPLICATION | 102 | 2.4 | 0 | 0 |
| REACTOME_3_UTR_MEDIATED_TRANSLATIONAL_REGULATION | 106 | 2.4 | 0 | 0 |
| REACTOME_SRP_DEPENDENT_COTRANSLATIONAL_PROTEIN_TARGETING_TO_MEMBRANE | 109 | 2.39 | 0 | 0 |
| HSIAO_HOUSEKEEPING_GENES | 387 | 2.34 | 0 | 0 |
| REACTOME_NONSENSE_MEDIATED_DECAY_ENHANCED_BY_THE_EXON_JUNCTION_COMPLEX | 107 | 2.31 | 0 | 0 |
| RHEIN_ALL_GLUCOCORTICOID_THERAPY_DN | 350 | 2.3 | 0 | 0 |
| REACTOME_INFLUENZA_LIFE_CYCLE | 136 | 2.27 | 0 | 0 |
| YAO_TEMPORAL_RESPONSE_TO_PROGESTERONE_CLUSTER_13 | 159 | 2.27 | 0 | 0 |
| REACTOME_METABOLISM_OF_MRNA | 210 | 2.22 | 0 | 0 |
| WONG_EMBRYONIC_STEM_CELL_CORE | 331 | 2.22 | 0 | 0 |
| REACTOME_METABOLISM_OF_RNA | 255 | 2.2 | 0 | 0 |
| MOOTHA_VOXPHOS | 85 | 2.17 | 0 | 0 |
| PECE_MAMMARY_STEM_CELL_UP | 136 | 2.17 | 0 | 0 |
| REACTOME_FORMATION_OF_THE_TERNARY_COMPLEX_AND_SUBSEQUENTLY_THE_43S_COMPLEX | 49 | 2.17 | 0 | 0 |
| BILANGES_SERUM_AND_RAPAMYCIN_SENSITIVE_GENES | 68 | 2.15 | 0 | 0 |
| TARTE_PLASMA_CELL_VS_PLASMABLAST_DN | 306 | 2.12 | 0 | 0 |
| REACTOME_ACTIVATION_OF_THE_MRNA_UPON_BINDING_OF_THE_CAP_BINDING_COMPLEX_AND_EIFS_AND_SUBSEQUENT_BINDING_TO_43S | 57 | 2.12 | 0 | 0 |
| KEGG_PARKINSONS_DISEASE | 112 | 2.12 | 0 | 0 |
| YAMASHITA_LIVER_CANCER_WITH_EPCAM_UP | 52 | 2.11 | 0 | 0 |
| WONG_MITOCHONDRIA_GENE_MODULE | 216 | 2.11 | 0 | 0 |
| DANG_MYC_TARGETS_UP | 139 | 2.11 | 0 | 0 |
| YAO_TEMPORAL_RESPONSE_TO_PROGESTERONE_CLUSTER_17 | 173 | 2.11 | 0 | 0 |
| KEGG_OXIDATIVE_PHOSPHORYLATION | 116 | 2.11 | 0 | 0 |
| MALONEY_RESPONSE_TO_17AAG_DN | 78 | 2.11 | 0 | 0 |
| REACTOME_RESPIRATORY_ELECTRON_TRANSPORT_ATP_SYNTHESIS_BY_CHEMIOSMOTIC_COUPLING_AND_HEAT_PRODUCTION_BY_UNCOUPLING_PROTEINS_ | 81 | 2.09 | 0 | 0 |
| CHIANG_LIVER_CANCER_SUBCLASS_UNANNOTATED_DN | 185 | 2.09 | 0 | 0 |
| REACTOME_METABOLISM_OF_PROTEINS | 422 | 2.08 | 0 | 0 |
| PAL_PRMT5_TARGETS_UP | 198 | 2.07 | 0 | 0 |
| PROVENZANI_METASTASIS_DN | 135 | 2.06 | 0 | 0 |
| TAKAO_RESPONSE_TO_UVB_RADIATION_UP | 86 | 2.06 | 0 | 0 |
| ENK_UV_RESPONSE_KERATINOCYTE_UP | 528 | 2.05 | 0 | 0 |
| CAIRO_HEPATOBLASTOMA_CLASSES_UP | 580 | 2.05 | 0 | 0 |
| TIEN_INTESTINE_PROBIOTICS_6HR_UP | 54 | 2.05 | 0 | 0 |
| STARK_PREFRONTAL_CORTEX_22Q11_DELETION_DN | 469 | 2.04 | 0 | 0 |
| WANG_TUMOR_INVASIVENESS_UP | 361 | 2.03 | 0 | 0 |
| LEE_LIVER_CANCER_SURVIVAL_DN | 166 | 2.03 | 0 | 0 |
| TIEN_INTESTINE_PROBIOTICS_24HR_UP | 537 | 2.03 | 0 | 0 |
| REACTOME_RESPIRATORY_ELECTRON_TRANSPORT | 65 | 2.01 | 0 | 0 |
| PENG_GLUTAMINE_DEPRIVATION_DN | 331 | 2 | 0 | 0 |
| PENG_LEUCINE_DEPRIVATION_DN | 183 | 2 | 0 | 0 |
| BOYAULT_LIVER_CANCER_SUBCLASS_G3_UP | 183 | 2 | 0 | 0 |
| LI_CISPLATIN_RESISTANCE_UP | 24 | 2 | 0 | 0 |
| BLUM_RESPONSE_TO_SALIRASIB_DN | 339 | 1.99 | 0 | 0 |
| BERENJENO_TRANSFORMED_BY_RHOA_UP | 519 | 1.99 | 0 | 0 |
| PUJANA_CHEK2_PCC_NETWORK | 762 | 1.99 | 0 | 0 |

| | | | | |
|---|---|---|---|---|
| REACTOME_TCA_CYCLE_AND_RESPIRATORY_ELECTRON_TRANSPORT | 117 | 1.98 | 0 | 0 |
| SWEET_KRAS_ONCOGENIC_SIGNATURE | 89 | 1.98 | 0 | 0 |
| ALONSO_METASTASIS_UP | 191 | 1.98 | 0 | 0 |
| KIM_BIPOLAR_DISORDER_OLIGODENDROCYTE_DENSITY_CORR_UP | 657 | 1.98 | 0 | 0 |
| YAO_TEMPORAL_RESPONSE_TO_PROGESTERONE_CLUSTER_14 | 135 | 1.96 | 0 | 0.001 |
| IRITANI_MAD1_TARGETS_DN | 46 | 1.96 | 0 | 0.001 |
| CHNG_MULTIPLE_MYELOMA_HYPERPLOID_UP | 52 | 1.95 | 0 | 0.001 |
| LI_DCP2_BOUND_MRNA | 87 | 1.95 | 0 | 0.001 |
| RHODES_UNDIFFERENTIATED_CANCER | 68 | 1.95 | 0 | 0.001 |
| ZAMORA_NOS2_TARGETS_UP | 66 | 1.95 | 0 | 0.001 |
| REACTOME_AUTODEGRADATION_OF_CDH1_BY_CDH1_APC_C | 56 | 1.94 | 0 | 0.001 |
| JIANG_AGING_HYPOTHALAMUS_UP | 46 | 1.94 | 0 | 0.001 |
| KEGG_HUNTINGTONS_DISEASE | 172 | 1.94 | 0 | 0.001 |
| HILLION_HMGA1B_TARGETS | 90 | 1.94 | 0 | 0.001 |
| LI_AMPLIFIED_IN_LUNG_CANCER | 175 | 1.94 | 0 | 0.001 |
| MOOTHA_HUMAN_MITODB_6_2002 | 421 | 1.93 | 0 | 0.001 |
| REACTOME_CYCLIN_E_ASSOCIATED_EVENTS_DURING_G1_S_TRANSITION_ | 62 | 1.93 | 0 | 0.001 |
| GRAHAM_CML_DIVIDING_VS_NORMAL_QUIESCENT_UP | 178 | 1.93 | 0 | 0.001 |
| BENPORATH_PROLIFERATION | 136 | 1.93 | 0 | 0.001 |
| BHATTACHARYA_EMBRYONIC_STEM_CELL | 88 | 1.93 | 0 | 0.001 |
| SHIPP_DLBCL_VS_FOLLICULAR_LYMPHOMA_UP | 44 | 1.92 | 0 | 0.001 |
| REACTOME_MITOTIC_G1_G1_S_PHASES | 130 | 1.92 | 0 | 0.001 |
| MENSSEN_MYC_TARGETS | 51 | 1.92 | 0 | 0.001 |
| MOREAUX_B_LYMPHOCYTE_MATURATION_BY_TACI_DN | 67 | 1.92 | 0 | 0.001 |
| KIM_ALL_DISORDERS_OLIGODENDROCYTE_NUMBER_CORR_UP | 731 | 1.92 | 0 | 0.001 |
| REACTOME_APC_C_CDH1_MEDIATED_DEGRADATION_OF_CDC20_AND_OTHER_APC_C_CDH1_TARGETED_PROTEINS_IN_LATE_MITOSIS_EARLY_G1 | 64 | 1.92 | 0 | 0.001 |
| REACTOME_CDK_MEDIATED_PHOSPHORYLATION_AND_REMOVAL_OF_CDC6 | 46 | 1.92 | 0 | 0.001 |
| PROVENZANI_METASTASIS_UP | 186 | 1.92 | 0 | 0.001 |
| SESTO_RESPONSE_TO_UV_C0 | 107 | 1.91 | 0 | 0.001 |
| REACTOME_REGULATION_OF_ORNITHINE_DECARBOXYLASE_ODC | 48 | 1.91 | 0 | 0.002 |
| REACTOME_APC_C_CDC20_MEDIATED_DEGRADATION_OF_MITOTIC_PROTEINS | 65 | 1.91 | 0 | 0.002 |
| REACTOME_ASSEMBLY_OF_THE_PRE_REPLICATIVE_COMPLEX | 63 | 1.91 | 0 | 0.002 |
| DAZARD_RESPONSE_TO_UV_SCC_UP | 114 | 1.91 | 0 | 0.002 |
| REACTOME_SCFSKP2_MEDIATED_DEGRADATION_OF_P27_P21 | 53 | 1.91 | 0 | 0.002 |
| ZHOU_TNF_SIGNALING_30MIN | 52 | 1.91 | 0 | 0.002 |
| MANALO_HYPOXIA_DN | 273 | 1.9 | 0 | 0.002 |
| SPIELMAN_LYMPHOBLAST_EUROPEAN_VS_ASIAN_UP | 469 | 1.9 | 0 | 0.002 |
| WEI_MYCN_TARGETS_WITH_E_BOX | 737 | 1.9 | 0 | 0.002 |
| REACTOME_SCF_BETA_TRCP_MEDIATED_DEGRADATION_OF_EMI1 | 49 | 1.9 | 0 | 0.002 |
| REACTOME_ER_PHAGOSOME_PATHWAY | 58 | 1.9 | 0 | 0.002 |
| SOTIRIOU_BREAST_CANCER_GRADE_1_VS_3_UP | 145 | 1.9 | 0 | 0.002 |
| REACTOME_VIF_MEDIATED_DEGRADATION_OF_APOBEC3G | 49 | 1.9 | 0 | 0.002 |
| REACTOME_REGULATION_OF_MITOTIC_CELL_CYCLE | 77 | 1.89 | 0 | 0.002 |
| REACTOME_G1_S_TRANSITION | 106 | 1.89 | 0 | 0.002 |
| GRADE_METASTASIS_DN | 43 | 1.89 | 0 | 0.002 |
| BILANGES_RAPAMYCIN_SENSITIVE_VIA_TSC1_AND_TSC2 | 71 | 1.89 | 0 | 0.002 |
| GRADE_COLON_AND_RECTAL_CANCER_UP | 275 | 1.89 | 0 | 0.002 |
| REACTOME_P53_INDEPENDENT_G1_S_DNA_DAMAGE_CHECKPOINT | 48 | 1.89 | 0 | 0.002 |
| REACTOME_ANTIGEN_PROCESSING_CROSS_PRESENTATION | 72 | 1.89 | 0 | 0.002 |
| KEGG_ALZHEIMERS_DISEASE | 156 | 1.89 | 0 | 0.002 |
| PENG_RAPAMYCIN_RESPONSE_DN | 238 | 1.89 | 0 | 0.002 |
| OUELLET_OVARIAN_CANCER_INVASIVE_VS_LMP_UP | 117 | 1.88 | 0 | 0.002 |
| CASORELLI_ACUTE_PROMYELOCYTIC_LEUKEMIA_DN | 643 | 1.88 | 0 | 0.003 |
| REACTOME_CDT1_ASSOCIATION_WITH_THE_CDC6_ORC_ORIGIN_COMPLEX | 54 | 1.88 | 0 | 0.003 |
| REACTOME_DESTABILIZATION_OF_MRNA_BY_AUF1_HNRNP_D0 | 50 | 1.88 | 0 | 0.003 |

| | | | | |
|---|---|---|---|---|
| REACTOME_M_G1_TRANSITION | 78 | 1.88 | 0 | 0.003 |
| JIANG_AGING_CEREBRAL_CORTEX_UP | 36 | 1.88 | 0 | 0.003 |
| BORCZUK_MALIGNANT_MESOTHELIOMA_UP | 296 | 1.87 | 0 | 0.003 |
| MOOTHA_MITOCHONDRIA | 434 | 1.87 | 0 | 0.003 |
| MORI_IMMATURE_B_LYMPHOCYTE_DN | 90 | 1.87 | 0 | 0.003 |
| KRIGE_RESPONSE_TO_TOSEDOSTAT_24HR_DN | 936 | 1.87 | 0 | 0.003 |
| HOLLMANN_APOPTOSIS_VIA_CD40_UP | 191 | 1.87 | 0 | 0.003 |
| NAKAMURA_TUMOR_ZONE_PERIPHERAL_VS_CENTRAL_UP | 270 | 1.86 | 0 | 0.003 |
| REACTOME_SIGNALING_BY_WNT | 62 | 1.86 | 0 | 0.003 |
| GRADE_COLON_CANCER_UP | 818 | 1.86 | 0 | 0.004 |
| BRIDEAU_IMPRINTED_GENES | 63 | 1.86 | 0 | 0.004 |
| REACTOME_CROSS_PRESENTATION_OF_SOLUBLE_EXOGENOUS_ANTIGENS_ENDOSOMES | 47 | 1.85 | 0 | 0.004 |
| REACTOME_AUTODEGRADATION_OF_THE_E3_UBIQUITIN_LIGASE_COP1 | 47 | 1.85 | 0 | 0.004 |
| DITTMER_PTHLH_TARGETS_UP | 111 | 1.85 | 0 | 0.004 |
| REACTOME_S_PHASE | 106 | 1.85 | 0 | 0.004 |
| ZHANG_RESPONSE_TO_CANTHARIDIN_DN | 67 | 1.85 | 0 | 0.005 |
| KEGG_METABOLISM_OF_XENOBIOTICS_BY_CYTOCHROME_P450 | 70 | 1.84 | 0 | 0.005 |
| NATSUME_RESPONSE_TO_INTERFERON_BETA_DN | 52 | 1.84 | 0 | 0.005 |
| TOOKER_GEMCITABINE_RESISTANCE_UP | 77 | 1.84 | 0 | 0.005 |
| ACEVEDO_LIVER_TUMOR_VS_NORMAL_ADJACENT_TISSUE_UP | 796 | 1.84 | 0 | 0.005 |
| CHAUHAN_RESPONSE_TO_METHOXYESTRADIOL_DN | 100 | 1.84 | 0 | 0.006 |
| KEGG_PROTEASOME | 44 | 1.83 | 0 | 0.006 |
| SESTO_RESPONSE_TO_UV_C7 | 68 | 1.83 | 0 | 0.006 |
| BIOCARTA_PROTEASOME_PATHWAY | 28 | 1.83 | 0 | 0.006 |
| REACTOME_SYNTHESIS_OF_DNA | 90 | 1.83 | 0 | 0.006 |
| REACTOME_REGULATION_OF_MRNA_STABILITY_BY_PROTEINS_THAT_BIND_AU_RICH_ELEMENTS | 81 | 1.83 | 0 | 0.006 |
| KIM_ALL_DISORDERS_DURATION_CORR_DN | 140 | 1.83 | 0 | 0.006 |
| CHANG_CORE_SERUM_RESPONSE_UP | 203 | 1.83 | 0 | 0.006 |
| SMID_BREAST_CANCER_RELAPSE_IN_PLEURA_DN | 25 | 1.83 | 0 | 0.006 |
| SANA_RESPONSE_TO_IFNG_DN | 83 | 1.83 | 0 | 0.006 |
| SCHLOSSER_MYC_TARGETS_REPRESSED_BY_SERUM | 154 | 1.82 | 0 | 0.006 |
| HONMA_DOCETAXEL_RESISTANCE | 32 | 1.81 | 0 | 0.007 |
| MUELLER_PLURINET | 299 | 1.81 | 0 | 0.007 |
| REACTOME_HOST_INTERACTIONS_OF_HIV_FACTORS | 120 | 1.81 | 0 | 0.007 |
| TONKS_TARGETS_OF_RUNX1_RUNX1T1_FUSION_MONOCYTE_UP | 198 | 1.81 | 0 | 0.007 |
| HU_ANGIOGENESIS_DN | 37 | 1.81 | 0 | 0.008 |
| WANG_SMARCE1_TARGETS_DN | 352 | 1.81 | 0 | 0.008 |
| DAZARD_RESPONSE_TO_UV_NHEK_UP | 237 | 1.81 | 0 | 0.008 |
| MISSIAGLIA_REGULATED_BY_METHYLATION_DN | 117 | 1.81 | 0 | 0.008 |
| REACTOME_PROTEIN_FOLDING | 51 | 1.81 | 0 | 0.008 |
| PRAMOONJAGO_SOX4_TARGETS_DN | 50 | 1.81 | 0 | 0.008 |
| PETROVA_PROX1_TARGETS_UP | 27 | 1.8 | 0 | 0.008 |
| SWEET_LUNG_CANCER_KRAS_UP | 475 | 1.8 | 0 | 0.008 |
| ROSTY_CERVICAL_CANCER_PROLIFERATION_CLUSTER | 137 | 1.8 | 0 | 0.008 |
| WANG_TNF_TARGETS | 23 | 1.8 | 0 | 0.008 |
| KORKOLA_EMBRYONIC_CARCINOMA_VS_SEMINOMA_UP | 21 | 1.8 | 0 | 0.008 |
| REACTOME_REGULATION_OF_APOPTOSIS | 56 | 1.8 | 0 | 0.008 |
| HUANG_DASATINIB_RESISTANCE_UP | 79 | 1.8 | 0 | 0.008 |
| HOLLEMAN_ASPARAGINASE_RESISTANCE_B_ALL_UP | 26 | 1.8 | 0 | 0.008 |
| HORIUCHI_WTAP_TARGETS_DN | 294 | 1.8 | 0 | 0.008 |
| CROONQUIST_NRAS_SIGNALING_DN | 72 | 1.8 | 0 | 0.009 |
| REACTOME_MITOTIC_M_M_G1_PHASES | 165 | 1.8 | 0 | 0.009 |
| WELCSH_BRCA1_TARGETS_UP | 194 | 1.79 | 0 | 0.009 |
| GARY_CD5_TARGETS_DN | 422 | 1.79 | 0 | 0.009 |
| ZHU_CMV_24_HR_UP | 93 | 1.79 | 0 | 0.009 |

| | | | | |
|---|---|---|---|---|
| FERRANDO_T_ALL_WITH_MLL_ENL_FUSION_DN | 87 | 1.79 | 0 | 0.009 |
| LUI_TARGETS_OF_PAX8_PPARG_FUSION | 34 | 1.79 | 0 | 0.009 |
| REACTOME_ORC1_REMOVAL_FROM_CHROMATIN | 65 | 1.79 | 0 | 0.009 |

**Table 6. List of primers used for Quantitative RT-PCR.**

Sequences of primers used for quantitative real time PCR.

| Target Gene | Primers | Sequences (5' to 3') | Probe |
|---|---|---|---|
| *EZH2* | Forward<br>Reverse | AGCTCCCGCTGAGGATGT<br>CAGTGTGCAGCCCACAAC | 25 |
| *EZH1* | Forward<br>Reverse | CATCCAGCGTGGACTTAAGAA<br>CGTTCTTCTGCACAGACTCCT | 62 |
| *E2F1* | Forward<br>Reverse | TACCTGGCCGAGAGCAGT<br>GGTGGTCAGATTCAGTGAGGT | 7 |
| *E2F2* | Forward<br>Reverse | AGGGGAAGTGCATCAGAGTG<br>CCAGCGAAGTGTCATACCG | 7 |
| *MYC* | Forward<br>Reverse | GCTGCTTAGACGCTGGATTT<br>TAACGTTGAGGGGCATCG | 66 |
| *NR4A1* | Forward<br>Reverse | ACAGCTTGCTTGTCGATGTC<br>GGTTCTGCAGCTCCTCCAC | 34 |
| *NR4A2* | Forward<br>Reverse | ATGAAGAGAGACGCGGAGAA<br>AAAAGCAATGGGGAGTCCA | 63 |
| *NR4A3* | Forward<br>Reverse | TCTCAGTGTTGGAATGGTAAAAGA<br>GGTTTGGAAGGCAGACGAC | 52 |
| *GAPDH* | Forward<br>Reverse | CTGACTTCAACAGCGACACC<br>TAGCCAAATTCGTTGTCATACC | 25 |

**Table 7. List of primers used for ChIP-PCR.**

Sequences of primers used for ChIP-PCR.

| Primer name | Primer sequence |
|---|---|
| EZH2-1 F[1] | GGAAGCCAAGTTTGAACCAG |
| EZH2-1 R[1] | GCGGTTAAAACCGTTACCAC |
| EZH2-2 F[2] | AACTCTGCGGCGCCGGTTCCCGCCAAGA |
| EZH2-2 R[2] | TTCGCTGTAAGGGACGCCACTGGCCGTGT |
| NR4A1-TSS+2-2 Fw | CCCTGAGGCTGTGTCTTCTT |
| NR4A1-TSS+2-2 Rv | TCCCAGTCTGTAGGGAGACG |

#1 Yu J, Yu J, Mani R-S, et al. An Integrated Network of Androgen Receptor, Polycomb, and TMPRSS2-ERG Gene Fusions in Prostate Cancer Progression. *Cancer cell* . 2010;17(5):443-454.

#2 Fujii S, Tokita K, Wada N, et al. MEK-ERK pathway regulates EZH2 overexpression in association with aggressive breast cancer subtypes. *Oncogene* . 2011;30(39):4118-4128.

**Clinical Cancer Research, 23, 16**

**Published on 15, August, 2017**

http://clincancerres.aacrjournals.org/content/23/16/4817.long